Primary Cilia Directionality Reveals a Slow Reverse Migration of Principal Neurons for Postnatal Positioning and Lamination in the Cerebral Cortex

Juan Yang[1,2], Soheila Mirhosseiniardakani[1,3], Liyan Qiu[1], Kostandina Bicja[1,3], Kevin Jungkai Lin[1,4], and Xuanmao Chen[1, *]

Department of Molecular, Cellular, and Biomedical Sciences[1]; the Graduate Programs in Biochemistry[2] or Genetics [3]; the Undergraduate Programs in Neuroscience and Behaviors[3] or Biomedical Sciences [4], University of New Hampshire, Durham, NH 03824

[*] Correspondence should be addressed to Dr. Xuanmao Chen: Department of Molecular, Cellular, and Biomedical Sciences, College of Life Sciences and Agriculture, University of New Hampshire, Rudman Hall Rm 389, 46 College Road, Durham, NH 03824. Phone: 603 862 4542, Fax: 603 862 4013, Email: Xuanmao.Chen@unh.edu.

Running Title: Primary Cilia and Principal Cell Positioning

Key Words: Neuronal Primary Cilia, Principal Cell Positioning, Cortical Lamination, Reverse Migration, Ift88 and Arl13b

Acknowledgments: This study was supported by National Institutes of Health Grants K01AG054729, P20GM113131-7006, R15MH126317, and R15MH125305 to X.C.; UNH CoRE PRP awards and Cole Neuroscience and Behavioral Faculty Research Awards to X.C.; UNH Summer TA Research Fellowships (STAF) and a Dissertation Year Fellowship (DYF) to J.Y. We would like to thank Brendon Lewis for helping analyze cilia directionality in the ventral CA1 region. We are grateful to the University Instrumentation Center at UNH for excellent A1R HD confocal imaging service.

Highlights

1. Primary cilia of early- and late-born CA1 neurons display opposite orientations, while primary cilia of neocortical principal neurons generally point towards one direction (the pial surface).
2. Late-born CA1 principal neurons, principal neurons in the neocortex, subiculum and postsubiculum undergo a reverse migration for postnatal cell positioning that helps shape cortical lamination.
3. Primary cilia orientation indicates the direction of reverse migration of principal neurons in the cerebral cortex.
4. Selective ablation of primary cilia in the forebrain leads to cortical expansion, altered lamination, and gyrification that is formed by the reverse migration of principal neurons.
5. Arl13b modulates the ciliation and postnatal positioning of hippocampal principal neurons.

Abstract

Currently little is known about the roles of neuronal primary cilia in postnatal neurodevelopment. Here we show that primary cilia of principal neurons in the cerebral cortex do not fully arise until the postnatal stage. Neuronal primary cilia undergo marked changes in morphology and orientation postnatally, concurrent with principal cell positioning. Primary cilia of early- and late-born hippocampal principal neurons display opposite orientations, while primary cilia of both early and late-born neocortical principal cells point toward one direction. In contrast, astrocytes and interneurons in the hippocampus, and neurons in nucleated brain regions do not display specific cilia directionality. Guided by the clue of cilia directionality, we discovered that principal neurons in the hippocampal CA1, subiculum, postsubiculum, and neocortex undergo a previously unnoticed, slow but substantial "reverse migration" for postnatal positioning and proper lamination. Further, selective disruption of primary cilia function in the forebrain using Ift88 or Arl13b conditional knockout mice leads to cortical expansion, altered cortical lamination, or gyrification in the retrosplenial cortex that is formed by reverse migration. Collectively, this work has identified reverse migration as a novel fundamental process for principal cell positioning that refines cortical lamination and gyrification in the cerebral cortex, and primary cilia orientation indicates the direction of reverse migration of principal neurons.

Key Words: Neuronal Primary Cilia, Principal Cell Positioning, Cortical Lamination, Reverse Migration, Cortical Gyrification, Postnatal Neurodevelopment, Ift88 and Arl13b

Introduction

Neuronal primary cilia are microtubule-based surface projections, which are widely expressed throughout the central nervous system [1-3]. They regulate various physiological functions including neurodevelopment, energy balance, and cognitive function [3-6]. Defects in primary cilia are associated with many types of brain disorders including neurodevelopmental disorders, obesity, and cognitive impairment [4, 6-11]. It is well-known that primary cilia modulate embryonic neurodevelopment [12, 13] by mediating the Sonic hedgehog (Shh) signaling [3, 4, 6, 14, 15], influencing cell fate specification in the ventral neural tube [16, 17], and forebrain neuronal patterning by regulating radial glia cell polarity [18-20]. Evidence also implicates primary cilia in neural circuit formation in the adult brain. For example, neuronal primary cilia modulate hippocampal memory by affecting adult neurogenesis [13, 21, 22]. A more recent study has shown that neuronal primary cilia and axons in the hippocampal CA1 region can form axo-ciliary synapses to short circuit neurotransmission [23]. However, the roles of neuronal primary cilia in the postnatal neurodevelopment are poorly understood.

Principal neurons in the cerebral cortex individually migrate from the germinal zone to their destinations via multiple steps [24-26]. One important step is the radial migration crawling along radial glial fibers [27]. The nuclear translocation of radial migration occurs in a saltatory manner, in which the centriole moves forward in the leading process, followed by nuclear translocation that is controlled by cytoskeleton dynamics [28-30]. The centriole is constantly connected to the nucleus through microtubule network [24, 27, 31-33]. Hence, the movements of the centriole and the nucleus are tightly coupled. It is known that the principal cell layer in the hippocampus and neocortex is subdivided into the deep and superficial sublayers along the radial axis [34, 35]. These two sublayers harbor early- and late-born principal neurons, respectively, which migrate to the hippocampal or cortical plate in a birthtime-dependent inside-out pattern [35, 36]. Following the radial migration that occurs primarily during embryonic stage [37, 38], principal neurons undergo a positioning step and subsequently become matured to develop synaptic connectivity [39, 40]. The first 2weeks after birth are the critical period for neuron positioning and neuronal maturation in the cerebral cortex, during which the mouse hippocampal superficial and deep sublayers gradually condense into a compact lamina [41], while the neocortical principal cell layer expands markedly to form 5 loose laminae (Layer II-VI) [42-45]. Although numerous studies have contributed to uncovering the cellular and molecular mechanisms of radial migration during embryonic development [24, 28, 36, 46-48], it remains to be elucidated how principal neurons in the cerebral cortex complete the positioning step during postnatal development.

Given that the centrioles lead the nuclear translocation of principal neurons during radial migration, primary cilia, after emanating from the mother centriole, may modulate or indicate soma position in the

cerebral cortex. We postulated that ciliation timing and cilia directionality could provide useful clues to reveal their function. Thus, we performed cilia morphology and directionality analyses. We first observed that primary cilia of principal neurons in the cerebral cortex do not prominently protrude out until the early postnatal stage. Neuronal primary cilia undergo marked changes in morphology and orientation, which coincides with the formation of synaptic connectivity or neuronal maturation in the hippocampus [49-52]. Intriguingly, primary cilia of early- and late-born hippocampal neurons display opposite directionality, while cilia of both early- and late-born neocortical neurons generally point towards the pial surface. Moreover, we discovered that the centrioles of CA1 late-born neurons migrate excessively to reach SP bottom and be clustered there before a reverse migration back to the main SP. This clue gradually led us to discover that principal neurons in many cortical regions, including the hippocampal CA1 (late-born neurons), subiculum, postsubiculum, neocortex, the cingulate or retrosplenial cortex, are subject to a slow but substantial reverse migration that help configurate specific laminae including gyrification during postnatal development. We further demonstrate that selective ablation of primary cilia in the forebrain using Ift88 flox/flox Emx1-Cre mice [53-55] not only causes a cortical expansion and altered cortical laminae, but also results in gyrification in the retrosplenial cortex. Intriguingly, this gyrification is formed through an invagination driven by cortical expansion and the reverse migration of late-born principal neurons. Consistently, selective shortening of primary cilia in the forebrain using Arl13b flox/flox Emx1-Cre mice [54, 56] also leads to altered lamination. Together, we identified a previously overlooked, slow but substantial "reverse migration" of principal neurons for postnatal positioning that helps shape cortical laminae including gyrification.

Results

Primary cilia of early- and late-born hippocampal CA1 neurons display opposite orientations.

To examine the morphological changes of neuronal primary cilia in SP during postnatal development, we performed immunofluorescence staining using AC3 [1, 57-59] and Arl13b antibodies [2, 60] on WT brain sections. We found that primary cilia morphology and orientation in SP underwent marked changes during early postnatal development (Fig. 1A-D). At P5 and P7, AC3- or Arl13b-positive neuronal primary cilia were rarely detected in the hippocampal SP (Fig. 1A). At P9, many neuronal primary cilia are visible but short and at P10, neuronal primary cilia were well elongated and became prominent, with many clustered at the edge of SP and SR (Fig. 1D). Interestingly, these primary cilia exhibited opposite orientations: the axoneme of primary cilia at the bottom (superficial sublayer) mostly pointed in the SR direction, whereas those at the top (deep sublayer) oriented toward the SO direction. From P9 to P14, cilia orientation underwent a drastic change (Fig. 1D). At P10, ~ 40% of cilia orientated toward SO (the north direction),

while at P14 nearly 20% of cilia pointed in the direction of SO (Fig. 1A-E). At P14, superficial-sublayer primary cilia occupied the major space of the SP, with the axonemes almost uniformly pointing in the SR direction. Deep-sublayer neurons were then squeezed to a thin layer at the top and their cilia kept an orientation towards SO. Note that at P14, most CA1 principal neurons have roughly completed the positioning step starting to form stable synapses [49, 50]. Afterwards at P40 and P75, cilia orientation did not change very much (Fig. 1E), except for becoming less uniformly in line with the radial axis (Fig. 1A). However, most primary cilia in the superficial sublayer were still aligned with the radial axis and oriented toward SR. Polar plots and histogram plots present changes in cilia orientation from P10 to P75 (Fig. 1C). It is noteworthy that the lamina thickness of SP decreased significantly from 95 µm at P3 to 60 µm at P40 (Fig. 1F) and continued to decrease with age (Fig. S1A). This suggests that pyramidal cells continue to adjust their position postnatally, which condenses the cell density when some neurons die [61], thereby decreasing CA1 lamina thickness.

To confirm if primary cilia with opposite orientation come from early- and late-born pyramidal neurons, respectively, we performed immunofluorescence staining using an antibody of calbindin, a marker for late-born neurons in the hippocampal CA1 after P20 [35, 62]. Fig. 1G shows that primary cilia of calbindin-positive neurons in the superficial sublayer largely pointed in the direction of SR, whereas calbindin-negative neurons' primary cilia generally oriented toward the SO direction, supporting the notion that early- and late-born pyramidal neurons exhibit opposite cilia orientations. To demonstrate early- and late-born neuron distribution in SP, we include *in situ* hybridization (ISH) results of Ndst4, Col11a1 and Htr1a, adopted from Allen Brain Atlas (https://mouse.brain-map.org/). Ndst4 and Col11a1 are markers of early-born pyramidal neurons [34], while Htr1a is selectively expressed in late-born neurons [35]. ISH data show that Ndst4 (Fig. S1A) and Col11a1 mRNA (Fig. S1B) were mostly detected in the deep sublayer, with a small fraction also distributing to the superficial sublayer, depending on age (Fig. S1A). Htr1a mRNA is identified largely in the superficial sublayer, whose staining signals cover the major but not all areas of the superficial sublayer (Fig. S1C). Together, these data demonstrate that primary cilia of early- and late-born hippocampal pyramidal neurons exhibit opposite orientation, suggesting a role of neuronal primary cilia in pyramidal cell positioning during postnatal development.

Arl13b regulates ciliation timing and cilia orientation in the hippocampal CA1 region.

We further observed that primary cilia marker AC3 expression in pyramidal cells in the hippocampal CA1 region remained relatively stable after P10 (Fig. 1A)[2]. In contrast, Arl13b started to emerge at P7 with staining identified strongly at the SP bottom (Fig. 1A). At P10, Arl13b expression reached a very high level in the SP, particularly strong at the SP bottom, then decreased at P14 and further faded away at P40

and diminished in adulthood (Fig. 1A). Arl13b high expression appears to occur within the same time-window as pyramidal cell positioning from ~P5 to P14 [49-51, 63], implicating in neuronal positioning. Arl13b is a ciliary small GTPase that modulates ciliogenesis, interneuron migration and maturation [20, 64, 65]. We have previously reported that Arl13b over-expression transgenic (Arl13b+) mice have much longer neuronal primary cilia in the hippocampus [60]. We further found that neuronal primary cilia of Arl13b+ mice are the longest in the hippocampal CA1 region, compared to many other brain regions including CA3, dentate gyrus, neocortex, and amygdala (Fig. S2). This highlights an important role of neuronal primary cilia in the CA1 region and of Arl13b in regulating neuronal cilia length.

To determine if Arl13b overexpression affects cilia development in the CA1 SP, we next characterized changes in cilia morphology and orientation during postnatal development using Arl13b+ mice and littermate controls. Firstly, we found that overexpression of Arl13b not only elongated primary cilia, but also affected the timing of ciliation (Fig. 2A-B and Fig. S3A). Arl13b+ mice started to express primary cilia in the deep sublayer as early as P3, all of which pointed toward SO (Fig. S3A). At P7, primary cilia of deep-sublayer neurons of Arl13b+ mice became quite long, while primary cilia of superficial-sublayer neurons were not fully elongated, with many remained dot-shaped at the bottom of SP (Fig. 2A). In addition, neuronal primary cilia of Arl13b+ mice were very different that of WT mice, whose cilia did not well arise yet (Fig. 2A). Deep-sublayer neuronal primary cilia of Arl13b+ largely pointed toward the SO direction, whereas primary cilia of superficial-sublayer neurons clearly show opposite cilia orientation (Fig. 2A-B). Secondly, immunostaining images from P7 to ~P75, polar and histogram plots of cilia orientation indicate that primary cilia in the hippocampal SP of Arl13b+ mice underwent drastic changes in orientation from P7 to P14 and mild changes from P14 to P75 (Fig. 2C-E), a pattern similar to that of WT mice. This suggests that the time-window before P14 is crucial for the changes in cilia orientation. Thirdly, overexpression of Arl13b affected the percentage of primary cilia having SO or SR orientation: at P14 and P40, more primary cilia pointed to the north in Arl13b+ mice than in WT mice (Fig. 2D-F). Lastly, we also used calbindin staining to verify that primary cilia with opposite orientation were indeed from early- and late-born pyramidal neurons, respectively (Fig. 2G). These data demonstrate significant changes in cilia orientation and strong effects of Arl13b in modulating CA1 ciliogenesis and cilia orientation during early postnatal development.

The observation that primary cilia of early-born neurons arise earlier than that of late-born neurons (Fig. 2 and S3A) raised the questions if early-born pyramidal neurons mature earlier than late-born neurons or if neuronal maturation and ciliation occur within the same time-window. To examine if there is a birthtime-dependent maturation in SP sublayers, we employed an antibody of NeuN, a protein marker for matured pyramidal neurons [66, 67], in our immunostaining assay. Fig. S3B shows that the expression of

NeuN was not detected at P1, except for some weak staining in the deep sublayer of SP. At P5, NeuN expression became stronger in the deep sublayer, but not much in the superficial sublayer. At P7, the superficial sublayer started to have higher NeuN expression, and at P14, NeuN was abundantly expressed in both deep- and superficial-sublayers. This "first deep - then superficial" sequential NeuN expression pattern indicates an order of birthtime-dependent neuronal maturation in the CA1 region. To determine if glutamatergic synaptic markers (indicative of synaptic connectivity) show a similar pattern, we searched Allen Brain Atlas Developing Mouse Brain (https://developingmouse.brain-map.org/). Indeed, we found that many synaptic marker proteins of glutamatergic synapses, including Shank3 (Fig. S3C), Homer-1 (Fig. S3D), Camk2a, PSD-95, Synapsin-1 and Syntaxin 1 (Table 1), display a similar sequential expression pattern: first expressed in the deep sublayer of SP at ~ P4, then extended to the superficial sublayer and reached full expression at P14 (Fig. S3 and Table 1). This expression sequence is in accordance with the order of primary cilia protrusion from P5 to P14 first in the deep and then superficial sublayer of the CA1 SP in both WT and Arl13b+ mice.

We also determined the cilia directionality in the hippocampal ventral CA1 region. Similarly, primary cilia of early- and late-born neurons in the ventral CA1 region of both WT and Arl13b+ mice clearly display opposite orientations at P9 (Fig. S4). The SR-pointing cilia orientation became more predominant from P9 to P40 (Fig. S4). However, the case in the hippocampal CA3 region is much different. Both WT and Arl13b+ had abundant expression of primary cilia at P5 and P7 in the deep and superficial sublayers of CA3 (Fig. S5), different from that of CA1 region (Fig. 1A). This indicates that CA3 protrudes neuronal primary cilia several days earlier than CA1. Coincidently, hippocampal CA3 pyramidal neurons mature several days earlier than CA1 neurons, as evidenced by NeuN expression pattern and strong expression of many glutamatergic synapse marker proteins including Camk2a and PSD-95 in the CA3 at P4 (Fig. S5 and Table 1). This sharply contrasts with the weak and deep sublayer-restricted expression in the dorsal CA1 region (Fig. S3 and Table 1). Allen Brain Atlas ISH data of other glutamatergic synapse markers also exhibit similar patterns (Table 1). These data suggest that neuronal ciliation in the hippocampus is somehow related to neuronal maturation, and neuronal ciliation in the CA1 SP coincides with neuronal maturation in an order of "first deep - then superficial".

Late-born Hippocampal CA1 Principal Neurons Undergo a Reverse Migration to Adjust Their Position Postnatally.

We observed that cilia orientation was changed from misaligned at P9 to very aligned at P14 (Fig. 1D), and cilia are clustered at the bottom of CA1 SP at P9-P10 in WT (Fig. 1) and P7 in Arl13b+ mice and then become more evenly distributed at P14 (Fig. 2). We postulated that cilia may reversely move from the

bottom of SP back to the main SP. To test it, we examined the centrioles/cilia distribution from P3 to P14 by utilizing Arl13b+ mice. We discovered that centriole density in the main SP of Arl13b+ mice at P3-P7 was very low (Fig. 3A), and a large fraction of centrioles/cilia was instead congregated at SP bottom, and not many centrioles are found in the middle panel of SP (Fig. 3A). However, a few days later, cilia distribution becomes more even in SP (Fig. 3A). This suggests that the centrioles/cilia of late-born principal neurons migrate excessively to reach and cluster at SP bottom before re-distribution. To test it, we quantified and compared nucleus density, centriole density, and the ratio of centriole to nucleus (C/N Ratio) in the CA1 SP at P3, P7, P10, and P14 using Arl13b+ mice (Fig. 3C-E). We manually separated confocal images of SP into top, middle, and bottom panels (Fig. 3B). We also included a section of SR (15 μm width) in the quantification because some centrioles further reached SR. First, we discovered that Arl13b+ mice do not show significant differences in nucleus density at the middle and bottom panels from P3 to P14 in the dorsal CA1 SP (Fig. 3C). However, centrioles are highly condensed at SP bottom at both P3 and P7 (Fig. 3D), and the C/N Ratio in SP bottom and SR are much higher than 1 (Fig. 3E). However, subsequently at P10 and P14, centrioles show a relatively even distribution in the whole SP (Fig. 3D). Consistently, C/N Ratio at P3 are about 2.5, but it gradually decreases to around 1 at P14 (Fig. 3E).

Cilia distribution changes from P3 to P14 also suggests that there is a reverse migration (from SP bottom back to main SP) in the superficial sublayer of CA1 SP. At P7, cilia density in the upper part of SP is very low, while short primary cilia are highly condensed at SP bottom (Fig. 3F). At P10, neuronal primary cilia were elongated. Some centrioles/cilia become well-aligned with the radial axis, while others still clustered at SP bottom (Fig. 3F), suggesting that some neurons start to move toward the north direction, and centrioles take the lead, followed by the hair-like cilia tails. At P14, long cilia occupied the major space of SP, and their primary cilia almost uniformly pointed in the SR direction (parallel to the radial glia fiber). There are no more centrioles/cilia clustering at SP bottom (Fig. 3F). This pattern was also observed in the WT mice (Fig. 1D). We also quantified cilia orientation of the upper part of SP, which originally only had SO-pointing cilia at P7. Due to this "pull-back" cilia/centriole migration, more south-oriented cilia gradually moved up to the main SP from P7 to P14, the upper part of SP subsequently contained more south-oriented cilia (Fig. 3G-H). It is well-known that individual principal neurons migrate to the hippocampal and neocortical plates along radial glia fibers in a saltatory manner, in which the centrosome moves forward in the leading process, followed by nuclear translocation driven by cytoskeleton dynamics[29, 30, 68]. Here, the cilia/centrioles of late-born principal neurons in the superficial sublayer in the hippocampal CA1 SP move against the radial migration direction to re-position back to the main CA1 SP (Fig. 3I). We name this postnatal positioning process "reverse migration". Given the thickness of SP reduced drastically, the reverse migration of centriole/cilia should concur with soma

re-positioning and backward movement. A schematic model depicts the process of postnatal cell positioning, and primary cilia orientations in the hippocampal CA1 region (Fig. 3I).

Principal Neurons in the Cerebral Cortex Move Backwards for Positioning and Lamination During Postnatal Development.

The hippocampal CA1 region and the neocortex share similarities in their neuronal migration mode and superficial-deep lamination during the embryonic stage (30, 50, 83). To examine whether the neocortex has similarities or distinctions to the hippocampal CA1 in term of ciliation pattern and principal cell positioning, we examined cilia protrusion timing, C/N ratio, and cilia orientation in the postnatal mouse neocortex (Fig. 4). We found that primary cilia are not protruded in the neocortical superficial sublayer until P7 (Fig. 4A-B). Similar to the CA1 region, neuronal primary cilia are expressed earlier in the deep sublayer than superficial sublayer in both WT and Arl13b+ mice (Fig. 4A-D). To determine if neocortical principal neurons are also subjected to a reverse migration as late-born hippocampal neurons in SP before P14, we examined centriole/nuclei distribution pattern in the superficial sublayer (Layer II/III) of the neocortex at P3 and P14 (Fig. 4E-H). For quantification, we drew top and middle panels on the images of Layer II/III to quantify centrioles and nuclei density (Fig. 4E). We found that the C/N ratios were near 1 and there were no significant differences between P3 and P14 and between the top and middle panels (Fig. 4F), suggesting that there is no excessive clustering of centrioles at Layer II/III in the neocortex. This is different from the result in the superficial sublayer of CA1 region (Fig. 3E). However, the density of nuclei (Fig. 4G) and centrioles (Fig. 4H) at the top panel were higher than those at the middle panel at P3. But at P14, both centriole and nuclei density between two panels had no significant differences. These data indicate that the densities of centrioles and nuclei in Layer II/III change from compact and uneven at P3 to sparse and even at P14, implying a reverse migration of soma. Consistently, the distances from the edge of the superficial sublayer to the pial surface gradually increase during the first two weeks after birth (Fig. 4I). Because neuronal primary cilia in the neocortex before P10 are too short to be quantified for directionality analysis (Fig. 4A-D), we thereby quantified cilia orientation in the neocortical sublayers using WT and Arl13b+ neocortical samples at P14 and P40 (Fig. 4J-K), when primary cilia of principal neurons in the cerebral cortex demonstrate a clear directionality. We found that primary cilia in the superficial sublayer of the neocortex orientate toward the pial surface in both WT and Arl13b+ mice, which is opposite to the direction of reverse migration. This phenomenon in the superficial layer is the same as what observed in the CA1 SP (Fig. 3E-G). In contrast, primary cilia in the deep sublayers of neocortex also point in the direction of pial surface, which is different from those in the CA1 SP.

We determined primary cilia directionality in other brain regions including subiculum and the piriform cortex. Generally, principal neurons in compact laminae in the cerebral cortex have opposite cilia directionality, while neurons in sparse laminae have uniform cilia directionality (Fig. S6, Table 2). We also compared cilia directionality in nucleated brain regions with laminated cortical regions. Primary cilia in the laminated cortical regions, such as the neocortex, hippocampal CA1, and subiculum, exhibit a clear directionality: they either have opposite cilia orientations or uniformly orientate towards the pial surface (Fig. S6). However, no clear cilia directionality was identified in the thalamus, amygdala, and hypothalamus (Fig. S6, Table 2), all of which are nucleated brain regions. We also examined the cilia directionality of interneurons and astrocytes in the hippocampus and neocortex. Primary cilia of interneurons and astrocytes exhibit irregular directionality (Fig. S6, Table 2). These data demonstrate that only principal neurons in laminated cortical regions display a marked cilia directionality. The clearest cilia directionality appears at P14 - P20 (Fig. 1-2 and Fig. S6), when principal neurons have generally completed the postnatal positioning procedure. Together, these suggest that it is the reverse migration of principal neurons during early postnatal neurodevelopment that causes neuronal primary cilia pointing towards a specific direction.

It is intriguing that primary cilia both in the deep and superficial sublayers of the neocortex point toward the pial surface (Fig. 4J-K). To confirm that principal cells in the neocortex indeed undergo slow reverse migration, we quantified the ratio of individual layer thickness relative to the whole six layers as well as the distance from Layer VI to the ventricular zone (VZ). We found that the thickness of superficial sublayer and deep sublayer changed drastically from E18.5 to P20. The superficial sublayer greatly expands, while the thickness of deep sublayer gradually reduced (Fig. 5A-D). In the meantime, the distance from the bottom of Layer VI to VZ significantly decreased with age postnatally (Fig. 5E-F). This data supports the interpretation that principal cells not only in the superficial but also the deep sublayer of the neocortex moves backward during early postnatal development.

To further verify that neocortical principal neurons undergo reverse migration during postnatal development, we developed a method that utilized CFSE dye to label cells in the outer layer of the neocortex at P0 and trace the location of labeled cells several days later. CFSE allows for rapid labeling of cells within 30 minutes and sustain visibility for several weeks within the brain, providing an excellent tool to trace neuron migration *in vivo* [38, 69-71]. Firstly, we found that CFSE dye stayed at the injection region, the outermost layer of the superficial sublayer at P1, while at P3, many CFSE-labeled superficial neurons appeared in inner layers, and further inside of the neocortex at P9 (Fig. 6A-B). This data demonstrate that CFSE-labels cells undergo reverse movement and migrate away from the pial surface. Because CFSE can label daughter cells[38, 72], EdU was also injected into E18.5 pregnant mice to label

new-born cells after E18.5. Our result show that those CFSE-labeled migrating cells were not merged with EdU (Fig. 6B), confirming that the CFSE-positive cells are not daughter cells of original labeled neurons. Secondly, to identify the cell type of reversely migrating cells, we utilized an antibody of Ctip2, an early-born principal neuron marker to stain CFSE-labeled brain samples. Interestingly, ~70% CFSE-labeled cells overlapped with Ctip2-marked cells (Fig. 6C-D). These data suggests that the CFSE-labeled neurons are mostly excitatory neurons. To rule out the possibility that CFSE may randomly diffuse into inner layers, we also injected CFSE into inner cortical layers and found that CFSE injected into inner layers did not spread to other regions (Fig. 6E). Together, these data confirm that principal neurons in the superficial sublayer of the neocortex undergo a backward movement during postnatal development.

We also examined if subiculum and postsubiculum, which are parahippocampal laminated region and right adjacent to the hippocampus[73], exhibit a similar reverse movement during early postnatal development by checking Allen Brain Atlas Developing Mouse Brain. We found that the demarcation between the distal CA1 and subiculum is not distinguishable at E18.5 and P4, but the compact CA1 - sparse subiculum distinction become prominent at P14 (Fig. S7, red arrows). This indicates that neurons in the subiculum, mostly early-born neurons based on Ctip2 staining, undergo a more drastic reverse migration than neurons in the CA1 SP. Moreover, the curvature in the postsubiculum was not remarkable at P4 but became obvious at P14 due to reverse migration (Fig. S7, bule arrows). Based on centriole backward movement (Fig. 1-3), CFSE cell tracing experiments (Fig. 6), lamination changes (Fig. 5 and S7), as well as additional ISH data from Allen Brain Atlas, we made a rough estimation on the speed of reverse migration at different cortical regions (Table 3). While there are regional variations, the reverse speed is more than 10 times slower than that typical radial migration. Nevertheless, during postnatal developmental course, the slow reverse migration can substantially impact lamina configuration (Fig. S7) (Table 3). Collectively, these data demonstrate that principal neurons in the cerebral cortex undergo a slow reverse movement for principal cell positioning during early postnatal development, and primary cilia orientations indicate the direction of the reverse migration.

Selective Disruption of Primary Cilia Function in the Forebrain Impacts Brain Size, Principal Cell Positioning and Lamination.

Next, we asked the question how primary cilia affect principal cell positioning. Evidence has shown that disruptions of cilia-related genes can cause microcephaly, macrocephaly and polymicrogyria (increased cortical folding)[74]. However, while most studies focus on elucidating the roles of primary cilia in the embryonic brain development, it is yet to be investigated how loss of primary cilia affect postnatal neurodevelopment. To selectively ablate or shorten primary cilia in the forebrain, we crossed Ift88 floxed

strain [54] and Arl13b floxed strain [56] with Emx1-cre mice, respectively, which expresses Cre selectively in the forebrain after E12.5[75]. Our immunostaining results confirmed that primary cilia in Ift88 flox/flox Emx1-cre conditional knockout (Ift88 cKO) mice were deleted in the cerebral cortex but not in other brain regions or non-neuronal organs (Fig. S8A-F). Similarly, primary cilia were shortened in the forebrain of Arl13b cKO mice (Fig. S8G-I). We utilized Ift88 cKO mice (Ift88 flox/flox Emx1-Cre) and Arl13b cKO (Arl13b flox/flox Emx1-Cre) mice to examine the effect of disruption of primary cilia function on postnatal development. We also included Arl13b+ mice, which have elongated primary cilia in the hippocampal region (Fig. S2), representing a mouse model of cilia gain-of-function.

To globally investigate gross structural changes in cilia KO brain, we used X-ray Micro-CT to scan the whole brains of P20 Ift88 cKO mice and littermate controls. Surprisingly, we first found that Ift88 cKO mice manifest gyrification in the granular retrosplenial cortex (RSG) or the cingulate neocortex (Fig. 7A) but not in other cortical regions. However, this regional gyrification was only observed in Ift88 cKO mice, not Arl13b cKO mice (not shown). Secondly, the cortical thickness of Ift88 cKO mice was slightly higher than controls at P20 (Fig. 7A-B). We quantified the brain weights of Ift88 cKO mice from P0 to adulthood. We discovered that Ift88 cKO mice did not show significant larger brain size in the embryonic stage (Fig. 7C), which is consistently with the published data[75]. They exhibited the most significant difference at P9 (Fig. 7C), when primary cilia are about to emanate (Fig. 1). Additionally, a low percentage of Ift88 cKO mice displayed spontaneous seizures 2 weeks after birth (Fig. 7D). Ift88 cKO mice exhibited cortical expansion, increased brain weight, and lower survival rate than controls, which together can be termed as megalencephaly. In contrast, Arl13b cKO mice only had slightly increased brain size at P9 but no significant difference at other ages (Fig. 7E). This indicates it is the ablation of primary cilia, not shortening, that causes megalencephaly in the early postnatal stage. Conversely, we discovered that the brain size of Arl13b+ mice before P9 was normal but had a smaller brain than controls after P14 (Fig. 7F), when primary cilia are already protruded. Those data suggest that the length of primary cilia can modulate ciliary signaling and influence postnatal neurodevelopment. We also examined neuronal composition in cortical layers by using Satb2 and Ctip2 antibodies, which are markers for late- and early-born neurons, respectively, to stain mouse brain sections. Due to megalencephaly, the neocortical outer layers of Ift88 cKO clearly had more neurons than controls (see Fig. 9A). More interesting phenotype was detected in Layer V, which is typically occupied by Ctip2-positive neurons (Fig. 7G-I). There was no difference in Ctip2 neuronal number in Layer V between Ift88 cKO and controls from P0 to adulthood (Fig. 7H). Nevertheless, Layer V of Ift88 cKOs had more Satb2-positive neurons after P5, but not at P0 or P3, than controls (Fig. 7I). Because typical radial migration is completed at P3, the difference in Layer V suggests that over-producing late-born Sabt2-positive neurons of Ift88 KOs first migrate to the outer

layer before P3 and then reversely migrate to the Layer V, thereby increasing the number of Sabt2-positive neurons in Layer V after P3. This is another piece of evidence supporting the concept of reverse migration.

Further, to examine how the gyrification in Ift88 cKO mice is formed in the cortex during postnatal development, we examined the development course of gyrification at different ages spanning from E18.5 to adulthood (Fig. 8A-C). We found that a shallow gyrus started to appear in RSG of Ift88 cKO mice at E18.5, and the degree of gyrification increased markedly from P0 to P9, and afterwards reached a steady state after P9 (Fig. 8A-C). Interestingly, this gyrus is formed through an invagination of the outer layer. Because continuously generated principal neurons near to the outer layer in the RSG are unable to move forward and squeezed in a confined area, this consequently leads to invagination caused by a reverse migration, therefore forming a sulcus. We further discovered that not only the degree of gyrification, but also the distance from the edge of Layer II to the midline is gradually increase with age, both of which are indicative of neuronal backward movement during postnatal development. Additionally, we measured the distance form Layer V (marked by Ctip2) to the midline in RSG. Consistently, we found that Layer V neurons in RSG continuously moved backward away from the midline, as indicated by the increased distance from Layer V to the midline. Together, these data provide additional evidence supporting the conclusion that cortical principal neurons move backwards away from the outer layers during postnatal development.

Next, we investigated the effects of cilia disruption on postnatal hippocampal neuron positioning. First, Ift88 cKO mice had abnormal CA1 SP compared to controls in the Satb2 and Ctip2 immunostaining (Fig. 9A-C). It is known that CA1 SP thickness gradually decreases with age (see Fig. S1A), partly due to cell apoptosis[76]. We discovered that ablation of primary cilia in Ift88 cKO mice caused delayed lamina condensation during P5-P9 (Fig. 9B-C), when primary cilia start to protrude primary cilia. Notably, the distal CA1 lamina thickness of Ift88 cKO mice had been impacted more strongly than that of the proximal CA1 (Fig. 9A&D). Consistently, Arl13b cKO mice, which lost cilia directionality in the CA1 (Fig. 9D), also have misplaced CA1 principal neurons both in the deep and superficial sublayers (Fig. 9F). This further supports the interpretation that primary cilia regulate the positioning of hippocampal principal neurons.

We also examined cilia directionality and morphology in the granular cell layer of dentate gyrus (DG). Primary cilia in the DG are relatively short (Fig. S2), thus we employed Centrin2-GFP mice, which mark the base of primary cilia in the granular cell layer, to identify cilia orientation in DG. We found that neuronal primary cilia in the granule cell layer are oppositely orientated at P14 (Fig. 10A-B), suggesting a role of primary cilia in modulating DG postnatal positioning. We also discovered that there was a developmental shift in Arl13b expression in primary cilia. Arl13b-labeled primary cilia are prominent at

P9, but become much weaker at P20 (Fig. 10C), when AC3-labled primary cilia became more predominant (Fig. 10C). We hypothesized that disruption of primary cilia function may affect neuronal positioning in the granule cell layer. Thus, we analyzed phenotypes in DG of Ift88 cKO and Arl13b cKO mice (Fig. 10D). We discovered that disruption of primary cilia function caused neuronal misplacement in the granular cell layer in DG in both Ift88 cKO and Arl13b cKO mice (Fig. 10E-G). The granular cell layer of both cKO mice lost the compactness. There were many individual Ctip2-positive neurons sparsely distributed in the outer molecular layer. Of note, the degree of misplaced neurons in the molecular layer in Arl13b cKO was lower than in Ift88 cKOs (Fig. 10G). These data support the hypothesis that primary cilia regulate the precise positioning of hippocampal principal neurons in the granular cell layer.

Discussion

This report presents multiple lines of evidence uncovering the roles of neuronal primary cilia in postnatal neurodevelopment: (1) The primary cilia of early- and late-born hippocampal neurons exhibit opposite orientations, whereas the primary cilia of both early- and late-born neocortical neurons point towards the pial surface. (2) We identify a previously unnoticed, slow but substantial “reverse migration” that late-born CA1 neurons, principal neurons in the neocortex, subiculum, and post-subiculum undergo in the first 2-3 weeks after birth for postnatal cell positioning, which refines various laminae in the cerebral cortex. (3) Neuronal primary cilia serve as a "compass" that indicates the direction of the reverse migration and postnatal positioning of principal neurons. (4) Selective ablation of primary cilia in the forebrain leads to cortical expansion, altered laminae, and cortical gyrification in the retrosplenial cortex, which generally manifest postnatally. (5) Cortical gyrification is formed through an invagination driven by cortical expansion and the reverse migration of principal cells. (6) Arl13b regulates the ciliation and postnatal positioning of hippocampal principal neurons.

The centriole, as the microtubule-organizing center, directs cellular microtubule dynamics that couple to nuclear translocation during cell migration (30, 33, 34, 92). Polarized centriole positioning is found to be important for properly oriented cell division, cilia positioning, and cell migration (93). Our findings suggest that primary cilia, after protruding from the mother centriole, modulate the positioning of early- and late-born principal neurons to the deep and superficial sublayers of the CA1 SP by influencing centriole migration and positioning (Fig. 1-3, S4). The interpretation is supported by evidence of genetic analyses. For example, selective ablation of primary cilia in the forebrain leads to altered lamination in the neocortex and hippocampal CA1 and DG (Fig. 7-10). Cilia shortening using Arl13b cKO mice manifests similar effects in the hippocampus (Fig. 9-10). Arl13b+ mice exhibit altered cilia pointing (Fig. 2F) and smaller brain (Fig. 7F). Currently, it is unknown how primary cilia exactly modulate

postnatal principal cell positioning. It is worth mentioning that primary cilia possess a highly conserved, rigid, 9+0 doublet axoneme architecture [77, 78], which are suited to generate, sense, or engage in cellular mechanical forces [78-84]. Primary cilia, after emanating from centrioles, may mechanically impede the fast saltatory migration of neurons [85]. After early- and late-born principal neurons migrate to reach the hippocampal plate, primary cilia first protrude out of early-born principal cells and point towards SO (Fig. 1-3), which is opposite to the principal neuron migration direction. This rigid protrusion may slow down the radial migration of early-born neurons and stabilize them in the deep sublayer. Likely due to delayed cilia protrusion, centrioles of late-born neurons excessively migrate a longer distance to reach the SP bottom, where they start to protrude primary cilia and then reverse (Fig. 3). It is not uncommon for primary cilia to engage in mechanical forces (39-45). For example, a recent study has shown that mechanical strain controls the length, motility, and planar position of primary cilia, affecting the determination of left-right body axis during gastrulation (94). We also have shown that olfactory cilia can sense mechanical force of airflow to regulate olfactory perception (95). Given the unique mechanical features of primary cilia, the differences in primary cilia protrusion and reverse movement may regulate centriole positioning in the cell and consequently affect principal cell positioning to the deep and superficial sublayers.

It is known that excitatory synaptic connectivity in the mouse hippocampus become matured in the first two weeks after birth (71-74). After hippocampal principal neurons reach the hippocampal plate via radial migration, it is unclear why they need to wait 2 weeks, instead of forming synapses immediately, to form matured synapses. We found that the centrioles of late-born neurons in CA1 SP undergo a striking reverse migration (over 10 - 35 μm) from P3 to P14 (Fig. 1-3). This could destabilize the cytoskeleton of dendrites and synapses, affecting the formation and stability of synaptic connections. This interpretation is in line with numerous reports showing that CA1 glutamatergic synapses before P14 are either silent or labile, and their electrophysiological features are different from mature synapses after P14. Likewise, neocortical Layer II/III late-born neurons also mature later than Layer V early-born neurons (ISH data of many synaptic markers available in the Allen Brain Atlas Developing Mouse Brain). In contrast, we did not observe marked reverse migration of CA3 neurons, and consistently CA3 principal neurons mature earlier that those in CA1 (Fig. S5). We have shown that CA1 principal neurons are subject to reverse migration for postnatal positioning during early postnatal development (Fig. 10 and Table 3). Likely the delayed synaptic maturation of late-born neurons could be, at least in part, explained by the reverse migration.

Our cilia directionality analyses led to the discovery of the reverse migration of principle neurons for postnatal cell positioning, which refine layered structures in the cerebral cortex during post neurodevelopment. We show that primary cilia of reversely migrating neurons display pointing that is

opposite to the direction of the reverse migration. For instance, primary cilia oriented oppositely in early- and late- born neurons in the compact CA1 SP (Fig. 1-2). In contrast, neuronal primary cilia in the neocortical deep and superficial sublayers exhibit a uniformed orientation (Fig. 4, S4, S6). We further demonstrate that principal neurons not only in the superficial sublayer but also the deep sublayer in the neocortex are subject to reverse migration for positioning during postnatal development (Fig. 5-6). In addition, the subiculum and postsubiculum also undergo reverse movement (Fig. S7). Primary cilia pointing within those area are opposite to the direction of reverse migration (Fig. S6B). Moreover, primary cilia orientation varies in regions of the brain. The brain is composed of both laminated and non-laminated structures. Laminar structures refer to regions of the brain that have distinct layers or laminae, typically found in the cerebral cortex. Non-laminar or nucleated structures do not possess distinct layers but instead have a nucleated organization. While primary cilia of principal neurons exhibit a directionality in laminated structures, they have an irregular orientation pattern in non-laminar structures (Fig. S6). In addition, primary cilia of interneurons and astrocytes do not display specific directionality, further supporting the notion that only principal neurons in layered structures display specific cilia directionality and it is the reverse migration of principal neurons that leads to cilia directionality.

One question arises why principal neurons need to undergo a reverse migration for postnatal cell positioning. The mammalian cerebral cortex, particularly the human neocortex, can be likened to a "library" consisting of numerous shelves and layers of "books" (principal neurons). The development of such a matrix-like architecture and its evolution from lower vertebrates to humans not only involves increased number of neurons and the needs of accommodating space (cortical expansion), program cell death, but also requires coordinated neuronal migration and precise cell positioning, as well as orderly neuronal maturation and circuit formation [45, 61, 86-88]. These processes are necessary for the brain to acquire external information during postnatal development and learning processes to gradually construct well-organized networks to enable efficient information processing, storage, and retrieval. After embryonic development or the completion of radial migration, neocortical laminae are still very thin, and its outermost layer remains compact (Fig. S9). Thus far, it is not well understood why the mouse hippocampal CA1 and other allocortices maintain highly compact, while neocortical layers are drastically expanded and become sparsely and evenly distributed during postnatal development. Radial migration and inside-out pattern may have limitations to construct expanded, loosely layered, orderly distributed cortical lamina spanning from the neocortex to subiculum (Fig. S9). An additional step of reverse migration may help address such a tissue.

We propose a working model (Fig. S9), in which the slow reverse migration of principal neurons, coupled with fast radial migration and inside-out lamination pattern, is required for orderly constructing

matrix-like architectures in the cerebral cortex. (1) In compact lamina such as the mouse CA1 SP, late-born CA1 principal neurons reverse, whereas early-born neurons do not. Early- and late-born CA1 neurons continuously move against each other, gradually condensing the lamina or decreasing the lamina thickness during postnatal development (Fig. S1A and 3I). (2) In the subiculum, mostly Ctip2-positive neurons move backward significantly, encountering little impedance from other neurons. Consequently, it develops into a sparse lamina which is very distinct from CA1 SP (Fig. S7). (3) In the neocortex, both early- and late-born neurons undergo marked reverse migration (Fig. 5-6), gradually expanding the lamina and forming sparse 5 principal cell layers (Layer II-VI). Consistently, neuronal primary cilia of early- and late-born neurons clearly have uniform cilia directionality at P20, pointing towards the pial surface (Table 3 and Fig. 4 and Fig. S6). (4) In confined cortical regions, such as the RSG or cingulate cortex, over-produced neurons in Ift88 cKO mice are driven by reverse migration to make an invagination and form a sulcus (Fig. 8). (5) We predict that other cortical structures such as mammalian olfactory cortex, allocortices of reptiles may share some principles, if not all, in postnatal positioning with the mouse CA1, thus cilia directionality analyses will help understand how these layers of allocortex are constructed. (5) We also predict that markedly expanded but loosely layered CA1 lamina of primates is likely shaped by significant reverse migration of principal neurons following the radial migration. Together, the reverse migration of principal neurons is of great significance and refine laminar configuration in different cortical regions.

One may wonder why the process of reverse migration of principal neurons has not been reported previously. Possible explanations include: (1) It is counter-intuitive and occurs postnatally after the radial migration is completed. (2) The reverse migration is very slow. We roughly estimated the speed of reverse movement to be 0.1-3 μm/hr, depending on regions (Table 3), which is 10-30 fold slower than typical radial migration*[89]* (Table 3). This slow postnatal movement can be easily overlooked. (3) It is a backward movement of the cell body of principal neuron, not the whole neuron or all processes. (4) Principal neurons generally move back from highly compact regions to less condense regions (Fig. 1D, 5A, 8A). The high density of cells may prevent the observation of the backward movement of individual neurons. (5) Not all neocortical neurons in the mouse neocortex migrate at one time (Fig. 6). Only a small portion of neurons in the outer layer slowly migrate backwards (Fig. 6). (6) *Ex vivo* or live-tissue imaging mostly uses mice as an experimental model, which do not have gyrification. Gyrification is formed by collective migration at one location (Fig. 8), that may be easier to observe if using primate tissues. (7) Although it is recognized that the gyrification in the primate neocortex is driven by cortical expansion or increased neurogenesis [90-92], the principles of gyrification are not clearly known [90, 91, 93]. We are the first to show that gyrification is, at least partly, caused by the reverse migration of principal neurons

clustered in the outer layer. While we have collected solid evidence to substantiate the concept of reverse migration, it should be acknowledged that direct live-cell imaging evidence is lacking. Direct visualization of postnatal reverse migration of principal neurons and elucidating its underlying molecular mechanisms will greatly advance our understanding of how principal cells complete postnatal positioning to refine cortical laminae, implicating in cortical development and evolution.

Materials and Methods

Mice

All experiments are performed using mice with C57BL/6j genetic background. Ift88 floxed mice (Stock No. 022409), Arl13b floxed mice (Stock No. 031077), and Emx1-Cre (Stock No. 005628) were purchased from the Jackson Laboratory (JAX). The Arl13b-mCherry Centrin2-GFP double transgenic mice (Stock No. 027967) were purchased from JAX and originally have C57Bl/6, BALB/c, and FVB/N mixed genetic background. The expression of Arl13b-mCherry and Centrin2-GFP are both driven by the pCAGGs promoter [60, 94, 95]. After importing to the Chen lab, we have backcrossed this strain with C57BL/6j mice for more than six generations to obtain uniform C57BL/6j background. The backcrossing has yielded three separate mouse lines: The backcrossing has also yielded three separate lines: one keeps as Arl13b-mCherry; Centrin2-GFP double transgenic mice (Arl13b+ mice), which will be used to mark primary cilia orientation. The other two are Arl13b-mCherry single and Centrin2-GFP single transgenic mice. Centrin2-GFP was used to mark centrioles which locate to the base of primary cilia. Mice were maintained on a 12-hour light/dark cycle at 22 °C and had access to food and water ad libitum. All animal procedures were approved by the Institutional Animal Care and Use Committee at the University of New Hampshire (UNH).

Brain Tissue Collection

Mice were deeply anesthetized with an intraperitoneal injection of ketamine and xylazine, and then were transcardially perfused with ice-cold 0.1 M phosphate buffer saline (PBS) followed by 4% paraformaldehyde (PFA) in 0.1 M PBS. Young pups (P0 - P7) were directly decapitated using a sharp surgical scissors. Mouse brains were extracted and then placed into 4% PFA overnight at 4 °C. The following day, brains were rinsed in 0.1 M PBS for 30 min at room temperature. P0-P5 mouse brains then were dehydrated by 30% sucrose in 0.1 M PBS overnight at 4°C. Finally, those tissue were embedded in O.C.T resin before being sectioned at -18 °C using a cryostat to a thickness of 30 µm. P7 - P75 mouse brains were coronal sectioned using Compresstome (Precisionary Instruments LLC, NC) to a thickness of 30 - 50 µm.

Immunofluorescence Staining

E18.5-P5 mouse brains were sliced and mounted on gelatin-coated slices for immunostaining procedure, while P7 – P75 brain sections were sliced and placed in 24-wells plate, staying afloat during the staining procedure. They were washed three times with 0.1 M PBS. Then they were washed in 0.2% Triton X-100 (vol/vol) in 0.1 M PBS for three times for 10 minutes at room temperature. Then they were blocked in blocking buffer (0.1M PBS containing 10% normal donkey serum (vol/vol), 2% bovine serum albumin (weight/vol), 0.2% Triton X-100 (vol/vol)) for one hour at room temperature. After that, slices were incubated with primary antibodies overnight at 4 °C in blocking buffer. After washing in 0.1 M PBS for three times for 10 minutes, slices were incubated with secondary antibodies for 2 hours at room temperature. Primary antibodies were rabbit anti-AC3 (1:10000, EnCor Biotechnology Inc., #RPCA-AC3), mouse anti-Arl13b (1:500, UC Davis clone N295B/66), mouse anti-calbindin (1:1000, Swant Switzerland, D-28K), rat anti-Ctip2 (1:500, Millipore-Sigma, MABE1045), rabbit anti-Satb2 (1:500, Abcam, ab92446), and mouse anti-NeuN (1:500, Millipore-Sigma, MAB377, clone A60). Secondary antibodies were Alexa Fluor 488-, 546-, or 647-conjugated (Invitrogen, La Jolla, CA). Finally, sections were counter-stained with DAPI (Southern Biotech, #OB010020) and images were acquired with confocal microscope (Nikon, A1R-HD), installed in the University Instrument Center at UNH.

Cilia Orientation Measurement

When a single primary cilium in WT mice was measured, the relatively thinner axoneme was defined as the tip and the opposite site as the base. For Arl13b-mCherry & Centrin2-GFP transgenic mice, the location of the primary cilium base was the same as Centrin2-GFP. The tails of most primary cilia in WT mice were straight and easy to determine their angles. However, primary cilia in the Arl13b-mCherry & Centrin2-GFP transgenic mice were much longer and showed kinks in their axoneme [60]. For those primary cilia, the initial part (~2 μm from the base) was used for determining the angle of those primary cilia. Fiji was utilized to measure the orientation of the single primary cilium. Four steps were used to complete a measurement. 1) First, the angle tool was selected among icons showed in the main window. 2) Then, the shift button on the keyboard was held, while left clicking the mouse meanwhile to draw a line (always from the right to left and parallel to the external capsule) to the location of the base of the primary cilium. 3) Afterwards, the shift button was released, and the mouse was left clicked to draw a line from the base to the tip of the primary cilium. 4) Lastly, while holding the control button and selecting "M" on the keyboard, the angle would jump out in a separate window. To measure the next primary cilium,

steps 2-4 were repeated. Acquired data were finally exported as an excel file and then to a MATLAB program, which was used to generate polar plots.

Primary Cilia Length Measurement

We measured the length of primary cilia based on published methods [96], with modifications. The freehand line tool within Fiji (ImageJ) was used to measure cilia length from the base of axoneme to the distal tip.

CA1 SP Thickness Estimation

Confocal images of 20 µm Z-stack were used for quantifying CA1 SP thickness for both WT, Arl13b+ mice and Control mice. The straight-line tool within Fiji was used to measure CA1 SP thickness from the top of SP to the bottom of SP based on nucleus staining [97]. Because the nuclei at the top and bottom edge of SP are not aligned to a straight line, this causes some variation of SP thickness. For young adult mice, we chose coronal sections at -1.9 mm posterior to Bregma to measure CA1 SP thickness. For young pups, we measured the thickness based on selected slices with hippocampal anatomic geometry similar to adult hippocampal sections. We acknowledge that our estimation method has limitations and stereotaxic accuracy needs to be improved. Nevertheless, it is known [97] that CA1 SP thickness decreases markedly with age, particularly during the first two weeks. We present CA1 SP thickness changes with ages to demonstrate that hippocampal principal cells maintain certain movement or re-positioning postnatally, yielding significant changes during early postnatal period (before P14) and mild adjustment afterwards.

Quantification of nucleus density, centriole density, and ratio of centriole to nucleus (C/N Ratio)

A 70 µm x 70 µm square box in SP was used for one single area quantification. The freehand line tool within Fiji was utilized to draw a line that matched the margin of the nucleus at the bottom of SP in the chosen box. This line was then vertically moved down 15 µm (to the SR direction) and up 15 µm (to the SO direction). The panel between two lines was defined as the bottom panel of SP for quantifying nucleus, centrioles, and C/N Ratio. The top line at the bottom panel of SP was further moved up 30 µm (to the SO direction). The area between the two lines (having a width of 30 µm) was defined as the middle panel of SP for the quantification of nuclei and centrioles. Since many centrioles were found to be clustered in the SR particularly in Arl13b+ mice, we also included a 15-µm-width area in the SR that was next to SP for quantification. Two Centrin2 dots were counted as one pair of centrioles, one DAPI separate round region were counted as one nucleus.

Normalized Brain Size/Weight

Due to the variation of maternal care and individual body sizes, the same batch of pups may have variations in body weights and brain size. Thus, control littermates, cilia KO mice, or Arl13b+ mice differed by less than 10% in body weight were used to compare their brain size. To normalize brain size at different ages, we first averaged the whole brain weights in controls from the same cage, then divided each mouse brain weight by this average number. Then a final normalized brain size for each mouse was completed.

Cortical Injection of CellTracer

CFDA-SE is carboxyfluorescein diacetate succinimidyl ester, whose acetyl group is responsible for the initial membrane permeability of the compound and is cleaved by intracellular esterases upon entry into the cell, giving rise to CFSE. CFSE is fluorescent and accumulates intracellularly and can maintain fluorescence for over one month. To label cells in the neocortex of neonatal pups, pups had 0.5 ul of 0.25 mM CFSE dye (Life Technologies, #C34572 and Dojindo Molecular Technologies, #C375) injected into the neocortex, covering the pial surface. The CFSE dye was colored with Fast Green to monitor successful injection. Pups were anesthetized by hypothermia by laying them on an ice bed (icebox filled with ice and cover it with aluminum foil. Anesthesia was assessed by the loss of movement. P0-1 pups would need 1–2 min to be anesthetized by laying it on top of the ice bed, P3 and P5 pups need 3–6 min on the ice bed[98]. The head of the anesthetized pup was placed in a head holder[99] and secured with a small piece of cloth tape. An injection needle or glass pipette which contained CFSE dye was inserted perpendicular to the cortical layer. CFSE dye was manually injected into the neocortex by slowly pushing the injection bottom on the pipette. If the injection was successful, the colored dye slowly spread under the skull skin. The whole injection procedure were less than 8 mins. Afterwards, pups were removed from the head holder and placed it inside the recovery box on top of a heating mat for 10 minutes to achieve the normal body temperature, before gently returning the injected pups to their mother with the bedding.

EdU Injection and Staining

EdU (5-ethynyl-2-deoxyuridine, Carbosynth, #: NE08701) was dissolved in saline at 1 mg/ml and stored at -20 °C. E18.5 pregnant mice were given one-time intraperitoneal injection of EdU (100 mg/kg). For staining EdU, fixed brain slices were permeabilized for 30 minutes in PBS + 0.2% Triton X-100, and rinsed in PBS for 10 minutes, and then incubated in the fresh cocktail (Tris-buffered saline (100 mM final, pH 7.6), CuSO4 (4 mM final, Acros #197730010), Sulfo-Cyanine 3 Azide (2-5 uM final, Lumiprobe,

#D1330), and fresh Sodium Ascorbate (100 mM final, freshly made each use, Acros, #352685000)) for 30-60 minutes. Lastly, rinsed brain slices 3 times in PBS for totally 30 minutes.

X-ray Micro-CT Scanning of Iodine-Stained Brains

Mice were anesthetized and transcardially perfused with ice-cold PBS, followed by ice-cold 4% PFA in PBS. Brain tissues were carefully dissected and post-fixed in 4% PFA in PBS for 3 days at 4ºC. Brains were dehydrated in ethanol grade series (30%, 50%, 70%, 80%, 90%) for 2 h followed by 7 days staining in 90% methanol plus 1% iodine solution at room temperature in a dark area (replace with fresh staining buffer every 2 days.). After staining, brains were rehydrated with 30% and 70% ethanol, for 1 hour each, at room temperature with mild agitation. Finally, brains samples were fixed in 1% agarose gel (Apex Bioresearch Products, #: 20-102GP) and placed in 5 ml tubes at 4ºC. All iodine-stained mouse brains were scanned using Zeiss 610 Versa X-Ray micro-CT scanner. The micro-CT scan was carried out in an air-conditioned cabinet at 80 kV acceleration voltage and 125 µA tube current, 0.16º rotation step through 360 degrees, giving rise to 2201 projections; no filter was used. Exposure time was 6 seconds, and 3 X-ray projections were acquired in each angle increment and averaged for reduction of noise. The achieved resolution was around 6 µm with isotropic voxels. Tomographic reconstruction was performed using Dragonfly 2020 software.

Quantification of misplaced Ctip2-stained neurons in DG

We quantified misplaced Ctip2-neurons in the molecular layer of DG as indicated in Fig. 10F. Fiji was utilized to count the cell numbers. Firstly, the freehand line was selected among icons showed in the main window, then drawing a line which almost adjoined and covered the full outmost edge of granule cell layer (GCL) in the top layer and selecting "M" on the keyboard. Next, drawing several lines which is 20 µm, 30 µm, 50 µm perpendicular to the first line. Then copying the first line and move it parallelly to the end point of those 20 µm, 30 µm, 50 µm lines. After finishing this area selection step, the Plugins > Analyze > Cell Counter was selected among icons showed in the main window, after cell counter window showed up, first initializing the image, and then counting.

Statistical and Software

Data were analyzed with Fiji, GraphPad Prism and MATLAB. Data was considered as statistically significant if $p < 0.05$ and values in the graph are expressed as mean ± standard error of the mean (SEM). Statistical analyses were conducted using ANOVA for multiple group comparison or Student's T-test with

a two-tailed distribution, as appropriate. If not otherwise indicated in the text or figure legends, N.S., Not Significant; * $p < 0.05$; ** $p < 0.01$; *** $p < 0.001$.

References:

1. Bishop, G.A., et al., *Type III adenylyl cyclase localizes to primary cilia throughout the adult mouse brain.* J Comp Neurol, 2007. **505**(5): p. 562-71.
2. Sterpka, A. and X. Chen, *Neuronal and astrocytic primary cilia in the mature brain.* Pharmacol Res, 2018. **137**: p. 114-121.
3. Singla, V. and J.F. Reiter, *The primary cilium as the cell's antenna: signaling at a sensory organelle.* Science, 2006. **313**(5787): p. 629-33.
4. Valente, E.M., et al., *Primary cilia in neurodevelopmental disorders.* Nat Rev Neurol, 2014. **10**(1): p. 27-36.
5. Lee, J.E. and J.G. Gleeson, *Cilia in the nervous system: linking cilia function and neurodevelopmental disorders.* Curr Opin Neurol, 2011. **24**(2): p. 98-105.
6. Guemez-Gamboa, A., N.G. Coufal, and J.G. Gleeson, *Primary cilia in the developing and mature brain.* Neuron, 2014. **82**(3): p. 511-21.
7. Lee, J.H. and J.G. Gleeson, *The role of primary cilia in neuronal function.* Neurobiol Dis, 2010. **38**(2): p. 167-72.
8. Houlden, H., et al., *Mutations in TTBK2, encoding a kinase implicated in tau phosphorylation, segregate with spinocerebellar ataxia type 11.* Nat Genet, 2007. **39**(12): p. 1434-6.
9. Goetz, S.C., K.F. Liem, Jr., and K.V. Anderson, *The spinocerebellar ataxia-associated gene Tau tubulin kinase 2 controls the initiation of ciliogenesis.* Cell, 2012. **151**(4): p. 847-858.
10. Bowie, E., et al., *Spinocerebellar ataxia type 11-associated alleles of Ttbk2 dominantly interfere with ciliogenesis and cilium stability.* PLoS Genet, 2018. **14**(12): p. e1007844.
11. Ikeuchi, Y., et al., *The XLID protein PQBP1 and the GTPase Dynamin 2 define a signaling link that orchestrates ciliary morphogenesis in postmitotic neurons.* Cell Rep, 2013. **4**(5): p. 879-89.
12. Hasenpusch-Theil, K. and T. Theil, *The Multifaceted Roles of Primary Cilia in the Development of the Cerebral Cortex.* Front Cell Dev Biol, 2021. **9**: p. 630161.
13. Park, S.M., H.J. Jang, and J.H. Lee, *Roles of Primary Cilia in the Developing Brain.* Front Cell Neurosci, 2019. **13**: p. 218.
14. Ruat, M., et al., *Hedgehog trafficking, cilia and brain functions.* Differentiation, 2012. **83**(2): p. S97-104.
15. Bangs, F. and K.V. Anderson, *Primary Cilia and Mammalian Hedgehog Signaling.* Cold Spring Harb Perspect Biol, 2017. **9**(5).
16. Pal, K. and S. Mukhopadhyay, *Primary cilium and sonic hedgehog signaling during neural tube patterning: role of GPCRs and second messengers.* Dev Neurobiol, 2015. **75**(4): p. 337-48.
17. Mukhopadhyay, S., et al., *The ciliary G-protein-coupled receptor Gpr161 negatively regulates the Sonic hedgehog pathway via cAMP signaling.* Cell, 2013. **152**(1-2): p. 210-23.
18. Dessaud, E., A.P. McMahon, and J. Briscoe, *Pattern formation in the vertebrate neural tube: a sonic hedgehog morphogen-regulated transcriptional network.* Development, 2008. **135**(15): p. 2489-503.
19. Gorivodsky, M., et al., *Intraflagellar transport protein 172 is essential for primary cilia formation and plays a vital role in patterning the mammalian brain.* Dev Biol, 2009. **325**(1): p. 24-32.
20. Higginbotham, H., et al., *Arl13b-regulated cilia activities are essential for polarized radial glial scaffold formation.* Nat Neurosci, 2013. **16**(8): p. 1000-7.
21. Amador-Arjona, A., et al., *Primary cilia regulate proliferation of amplifying progenitors in adult hippocampus: implications for learning and memory.* J Neurosci, 2011. **31**(27): p. 9933-44.

22. Breunig, J.J., et al., *Primary cilia regulate hippocampal neurogenesis by mediating sonic hedgehog signaling.* Proc Natl Acad Sci U S A, 2008. **105**(35): p. 13127-32.
23. Sheu, S.H., et al., *A serotonergic axon-cilium synapse drives nuclear signaling to alter chromatin accessibility.* Cell, 2022. **185**(18): p. 3390-3407 e18.
24. Marin, O., et al., *Guiding neuronal cell migrations.* Cold Spring Harb Perspect Biol, 2010. **2**(2): p. a001834.
25. Marin, O. and J.L. Rubenstein, *Cell migration in the forebrain.* Annu Rev Neurosci, 2003. **26**: p. 441-83.
26. Hatten, M.E., *Central nervous system neuronal migration.* Annu Rev Neurosci, 1999. **22**: p. 511-39.
27. Tsai, L.H. and J.G. Gleeson, *Nucleokinesis in neuronal migration.* Neuron, 2005. **46**(3): p. 383-8.
28. Rahimi-Balaei, M., et al., *Neuronal Migration During Development of the Cerebellum.* Front Cell Neurosci, 2018. **12**: p. 484.
29. Kuijpers, M. and C.C. Hoogenraad, *Centrosomes, microtubules and neuronal development.* Mol Cell Neurosci, 2011. **48**(4): p. 349-58.
30. Higginbotham, H.R. and J.G. Gleeson, *The centrosome in neuronal development.* Trends Neurosci, 2007. **30**(6): p. 276-83.
31. Rivas, R.J. and M.E. Hatten, *Motility and cytoskeletal organization of migrating cerebellar granule neurons.* J Neurosci, 1995. **15**(2): p. 981-9.
32. Kawauchi, T., *Cellullar insights into cerebral cortical development: focusing on the locomotion mode of neuronal migration.* Front Cell Neurosci, 2015. **9**: p. 394.
33. Xie, Z., et al., *Serine 732 phosphorylation of FAK by Cdk5 is important for microtubule organization, nuclear movement, and neuronal migration.* Cell, 2003. **114**(4): p. 469-82.
34. Cembrowski, M.S. and N. Spruston, *Heterogeneity within classical cell types is the rule: lessons from hippocampal pyramidal neurons.* Nat Rev Neurosci, 2019. **20**(4): p. 193-204.
35. Soltesz, I. and A. Losonczy, *CA1 pyramidal cell diversity enabling parallel information processing in the hippocampus.* Nat Neurosci, 2018. **21**(4): p. 484-493.
36. Khalaf-Nazzal, R. and F. Francis, *Hippocampal development - old and new findings.* Neuroscience, 2013. **248**: p. 225-42.
37. Kriegstein, A.R. and S.C. Noctor, *Patterns of neuronal migration in the embryonic cortex.* Trends Neurosci, 2004. **27**(7): p. 392-9.
38. Yoshinaga, S., et al., *Comprehensive characterization of migration profiles of murine cerebral cortical neurons during development using FlashTag labeling.* iScience, 2021. **24**(4): p. 102277.
39. Moffat, J.J., et al., *Genes and brain malformations associated with abnormal neuron positioning.* Mol Brain, 2015. **8**(1): p. 72.
40. Liu, X., et al., *NONO Regulates Cortical Neuronal Migration and Postnatal Neuronal Maturation.* Neurosci Bull, 2019. **35**(6): p. 1097-1101.
41. Yang, J., L. Qiu, and X. Chen, *Neuronal primary cilia regulate pyramidal cell positioning to the deep and superficial sublayers in the hippocampal CA1.* BioRxiv, 2021.
42. Wiesel, T.N., *Postnatal development of the visual cortex and the influence of environment.* Nature, 1982. **299**(5884): p. 583-91.
43. Schwartz, M.L. and P. Goldman-Rakic, *Development and plasticity of the primate cerebral cortex.* Clin Perinatol, 1990. **17**(1): p. 83-102.
44. Danka Mohammed, C.P. and R. Khalil, *Postnatal Development of Visual Cortical Function in the Mammalian Brain.* Front Syst Neurosci, 2020. **14**: p. 29.
45. Geschwind, D.H. and P. Rakic, *Cortical evolution: judge the brain by its cover.* Neuron, 2013. **80**(3): p. 633-47.
46. Cooper, J.A., *A mechanism for inside-out lamination in the neocortex.* Trends Neurosci, 2008. **31**(3): p. 113-9.

47. Reiner, O., *LIS1 and DCX: Implications for Brain Development and Human Disease in Relation to Microtubules.* Scientifica (Cairo), 2013. **2013**: p. 393975.
48. Silva, C.G., E. Peyre, and L. Nguyen, *Cell migration promotes dynamic cellular interactions to control cerebral cortex morphogenesis.* Nat Rev Neurosci, 2019. **20**(6): p. 318-329.
49. Fiala, J.C., et al., *Synaptogenesis via dendritic filopodia in developing hippocampal area CA1.* J Neurosci, 1998. **18**(21): p. 8900-11.
50. Lauri, S.E., et al., *Functional maturation of CA1 synapses involves activity-dependent loss of tonic kainate receptor-mediated inhibition of glutamate release.* Neuron, 2006. **50**(3): p. 415-29.
51. Thakar, S., et al., *Evidence for opposing roles of Celsr3 and Vangl2 in glutamatergic synapse formation.* Proc Natl Acad Sci U S A, 2017. **114**(4): p. E610-E618.
52. Hsia, A.Y., R.C. Malenka, and R.A. Nicoll, *Development of excitatory circuitry in the hippocampus.* J Neurophysiol, 1998. **79**(4): p. 2013-24.
53. Gorski, J.A., et al., *Cortical excitatory neurons and glia, but not GABAergic neurons, are produced in the Emx1-expressing lineage.* J Neurosci, 2002. **22**(15): p. 6309-14.
54. Haycraft, C.J., et al., *Intraflagellar transport is essential for endochondral bone formation.* Development, 2007. **134**(2): p. 307-16.
55. Berbari, N.F., et al., *Hippocampal and cortical primary cilia are required for aversive memory in mice.* PLoS One, 2014. **9**(9): p. e106576.
56. Su, C.Y., et al., *Temporal deletion of Arl13b reveals that a mispatterned neural tube corrects cell fate over time.* Development, 2012. **139**(21): p. 4062-71.
57. Chen, X., et al., *Ablation of Type III Adenylyl Cyclase in Mice Causes Reduced Neuronal Activity, Altered Sleep Pattern, and Depression-like Phenotypes.* Biol Psychiatry, 2016. **80**(11): p. 836-848.
58. Yang, J., et al., *Acid-Sensing Ion Channels Contribute to Type III Adenylyl Cyclase-Independent Acid Sensing of Mouse Olfactory Sensory Neurons.* Mol Neurobiol, 2020.
59. Zhou, Y., et al., *Comparative Phosphoproteomic Profiling of Type III Adenylyl Cyclase Knockout and Control, Male, and Female Mice.* Front Cell Neurosci, 2019. **13**: p. 34.
60. Sterpka, A., et al., *Diverged morphology changes of astrocytic and neuronal primary cilia under reactive insults.* Mol Brain, 2020. **13**(1): p. 28.
61. Wong, F.K. and O. Marin, *Developmental Cell Death in the Cerebral Cortex.* Annu Rev Cell Dev Biol, 2019. **35**: p. 523-542.
62. Valero, M., et al., *Determinants of different deep and superficial CA1 pyramidal cell dynamics during sharp-wave ripples.* Nat Neurosci, 2015. **18**(9): p. 1281-1290.
63. Radic, T., et al., *Differential Postnatal Expression of Neuronal Maturation Markers in the Dentate Gyrus of Mice and Rats.* Front Neuroanat, 2017. **11**: p. 104.
64. Larkins, C.E., et al., *Arl13b regulates ciliogenesis and the dynamic localization of Shh signaling proteins.* Mol Biol Cell, 2011. **22**(23): p. 4694-703.
65. Gigante, E.D., et al., *ARL13B regulates Sonic hedgehog signaling from outside primary cilia.* Elife, 2020. **9**.
66. Sarnat, H.B., D. Nochlin, and D.E. Born, *Neuronal nuclear antigen (NeuN): a marker of neuronal maturation in early human fetal nervous system.* Brain Dev, 1998. **20**(2): p. 88-94.
67. Gusel'nikova, V.V. and D.E. Korzhevskiy, *NeuN As a Neuronal Nuclear Antigen and Neuron Differentiation Marker.* Acta Naturae, 2015. **7**(2): p. 42-7.
68. Rahimi-Balaei, M., et al., *Neuronal Migration During Development of the Cerebellum.* Frontiers in Cellular Neuroscience, 2018. **12**(484).
69. Telley, L., et al., *Sequential transcriptional waves direct the differentiation of newborn neurons in the mouse neocortex.* Science, 2016. **351**(6280): p. 1443-6.
70. Govindan, S., P. Oberst, and D. Jabaudon, *In vivo pulse labeling of isochronic cohorts of cells in the central nervous system using FlashTag.* Nat Protoc, 2018. **13**(10): p. 2297-2311.

71. Stoufflet, J., et al., *Primary cilium-dependent cAMP/PKA signaling at the centrosome regulates neuronal migration.* Sci Adv, 2020. **6**(36).
72. Telley, L., et al., *Sequential transcriptional waves direct the differentiation of newborn neurons in the mouse neocortex.* Science, 2016. **351**(6280): p. 1443-1446.
73. van Strien, N.M., N.L.M. Cappaert, and M.P. Witter, *The anatomy of memory: an interactive overview of the parahippocampal–hippocampal network.* Nature Reviews Neuroscience, 2009. **10**(4): p. 272-282.
74. Zaidi, D., K. Chinnappa, and F. Francis, *Primary Cilia Influence Progenitor Function during Cortical Development.* Cells, 2022. **11**(18).
75. Snedeker, J., et al., *Unique spatiotemporal requirements for intraflagellar transport genes during forebrain development.* PLOS ONE, 2017. **12**(3): p. e0173258.
76. Pönniö, T. and O.M. Conneely, *nor-1 regulates hippocampal axon guidance, pyramidal cell survival, and seizure susceptibility.* Mol Cell Biol, 2004. **24**(20): p. 9070-8.
77. Satir, P. and S.T. Christensen, *Overview of structure and function of mammalian cilia.* Annu Rev Physiol, 2007. **69**: p. 377-400.
78. Ishikawa, T., et al., *Cilia and centrosomes: Ultrastructural and mechanical perspectives.* Semin Cell Dev Biol, 2021. **110**: p. 61-69.
79. Khayyeri, H., S. Barreto, and D. Lacroix, *Primary cilia mechanics affects cell mechanosensation: A computational study.* J Theor Biol, 2015. **379**: p. 38-46.
80. Bezares-Calderon, L.A., J. Berger, and G. Jekely, *Diversity of cilia-based mechanosensory systems and their functions in marine animal behaviour.* Philos Trans R Soc Lond B Biol Sci, 2020. **375**(1792): p. 20190376.
81. Resnick, A. and U. Hopfer, *Force-response considerations in ciliary mechanosensation.* Biophys J, 2007. **93**(4): p. 1380-90.
82. Prasad, R.M., X. Jin, and S.M. Nauli, *Sensing a sensor: identifying the mechanosensory function of primary cilia.* Biosensors (Basel), 2014. **4**(1): p. 47-62.
83. Spasic, M. and C.R. Jacobs, *Primary cilia: Cell and molecular mechanosensors directing whole tissue function.* Semin Cell Dev Biol, 2017. **71**: p. 42-52.
84. Shinohara, K., et al., *Two rotating cilia in the node cavity are sufficient to break left-right symmetry in the mouse embryo.* Nat Commun, 2012. **3**: p. 622.
85. Matsumoto, M., et al., *Dynamic Changes in Ultrastructure of the Primary Cilium in Migrating Neuroblasts in the Postnatal Brain.* J Neurosci, 2019. **39**(50): p. 9967-9988.
86. Franchini, L.F., *Genetic Mechanisms Underlying Cortical Evolution in Mammals.* Front Cell Dev Biol, 2021. **9**: p. 591017.
87. Karten, H.J., *Vertebrate brains and evolutionary connectomics: on the origins of the mammalian 'neocortex'.* Philos Trans R Soc Lond B Biol Sci, 2015. **370**(1684).
88. Karten, H.J. and T. Shimizu, *The origins of neocortex: connections and lamination as distinct events in evolution.* J Cogn Neurosci, 1989. **1**(4): p. 291-301.
89. Tabata, H. and K. Nakajima, *Multipolar Migration: The Third Mode of Radial Neuronal Migration in the Developing Cerebral Cortex.* The Journal of Neuroscience, 2003. **23**(31): p. 9996-10001.
90. Ronan, L., et al., *Differential tangential expansion as a mechanism for cortical gyrification.* Cereb Cortex, 2014. **24**(8): p. 2219-28.
91. Ronan, L. and P.C. Fletcher, *From genes to folds: a review of cortical gyrification theory.* Brain Struct Funct, 2015. **220**(5): p. 2475-83.
92. Fernandez, V. and V. Borrell, *Developmental mechanisms of gyrification.* Curr Opin Neurobiol, 2023. **80**: p. 102711.
93. Tallinen, T., et al., *Gyrification from constrained cortical expansion.* Proc Natl Acad Sci U S A, 2014. **111**(35): p. 12667-72.

94. Bangs, F.K., et al., *Lineage specificity of primary cilia in the mouse embryo.* Nat Cell Biol, 2015. **17**(2): p. 113-22.
95. Higginbotham, H., et al., *Transgenic mouse line with green-fluorescent protein-labeled Centrin 2 allows visualization of the centrosome in living cells.* Transgenic Res, 2004. **13**(2): p. 155-64.
96. Sipos, E., S. Komoly, and P. Acs, *Quantitative Comparison of Primary Cilia Marker Expression and Length in the Mouse Brain.* J Mol Neurosci, 2018. **64**(3): p. 397-409.
97. Ponnio, T. and O.M. Conneely, *nor-1 regulates hippocampal axon guidance, pyramidal cell survival, and seizure susceptibility.* Mol Cell Biol, 2004. **24**(20): p. 9070-8.
98. Oomoto, I., et al., *Protocol for cortical-wide field-of-view two-photon imaging with quick neonatal adeno-associated virus injection.* STAR Protoc, 2021. **2**(4): p. 101007.
99. Olivetti, P.R., C.O. Lacefield, and C. Kellendonk, *A device for stereotaxic viral delivery into the brains of neonatal mice.* 2020. **69**(4): p. 307-312.
100. Oshima, K., et al., *A Unique "Reversed" Migration of Neurons in the Developing Claustrum.* The Journal of Neuroscience, 2023. **43**: p. 693 - 708.
101. Borrell, V., et al., *In vivo Evidence for Radial Migration of Neurons by Long-Distance Somal Translocation in the Developing Ferret Visual Cortex.* Cerebral Cortex, 2005. **16**(11): p. 1571-1583.

Figure Legends:

Fig. 1. Opposite primary cilia orientation in the deep and superficial sublayers of in the CA1 SP. (A) Primary cilia morphology and orientation are subject to marked change with ages from P5 to ~P75. Scale bars: 10 µm. **(B)** A diagram showing cilia orientation measurement in the dorsal hippocampal CA1 SP. Cilia shown in the SP are posited in the polar plot on the bottom. Polar plot analyses were performed to determine primary cilia orientation distribution. The numbers (0-360º) on the out circles denote the degree of cilia orientation relative to the external capsule, and the numbers on concentric circles are the percentage of cilia orientation at specific angles. **(C)** Most primary cilia point in the SR direction (180º - 360º) in polar plots (Left). The histogram plots (binned in 10-degree intervals) present the percentage of cilia at different angles. The degrees in polar plots were converted to histogram plots by subtracting 180º. **(D)** Primary cilia abundantly emerged in the SP bottom at ~P9, and their distribution and directionality drastically changed from P9 to P14. Cyan arrows indicate the direction of cilia distribution (from the bottom to the top). Scale bars: 20 µm. **(E)** The percentage of north-oriented cilia decreased significantly from P10 to P40. **(F)** The thickness of SP lamina in the hippocampal CA1 decreases significantly from P3 - P75. Each triangle (in E-F) represents one location in SP for quantification. One-way ANOVA with Bonferroni's multiple comparison test. **(G)** Primary cilia of calbindin-positive neurons at P40 mostly orientate toward the SR direction, while calbindin-negative neurons' cilia generally point in the SO direction. The white boxes are enlarged at the bottom. Super: superficial sublayer; Deep, deep sublayer. P7: Postnatal Day 7; SP: stratum pyramidale; SO: stratum oriens; SR: stratum radiatum.

Fig. 2. Opposite primary cilia orientation in the hippocampal SP of Arl13b+ mice. (A) Early-born neurons in the deep sublayer protrude cilia earlier than neurons in the superficial sublayers at P3 for both WT mice and Arl13b+ mice, and those early-protruding cilia point towards the north. **(A-B)** At P7, WT (left) have few cilia in SP. Nevertheless, at P10 cilia are abundantly expressed. Transgenic expression of Arl13b in Arl13b+ mice (right) elongates cilia length and promotes earlier cilia expression. Cilia in the deep-layer point towards SO, whereas cilia in superficial sublayer point toward SR. **(C)** Primary cilia orientation changes at P7, P10, and P14. White boxes are enlarged at the bottom. White arrows indicate the mother centriole or the base of cilium, green arrows denote some Centrin2-GFP artifacts. Scale bars: 10 µm top, zoom in 5 µm at the bottom. **(D)** Polar plots and histogram plots of cilia orientation of Arl13b+ mice from P7-P75. **(E)** The percentage of north-oriented cilia at different ages of Arl13b+ mice. One-way ANOVA with Bonferroni's multiple comparison test. (F) The percentage of north-oriented cilia in WT compared to ARl13b+ mice. Each triangle represents the percentage of north-oriented cilia from an area of CA1 SP for quantifying cilia orientation (E-F). **(G)** Primary cilia of calbindin-positive neurons (purple) at P40 Arl13b+ mice also mostly pointed in the SR direction, while calbindin-negative neurons' cilia generally point in the SO direction. The white boxes are enlarged at the bottom.

Fig. 3. Centriole/cilia of late-born neurons are clustered at hippocampal SP bottom before a reverse migration. (A) Arl13b+ mice displayed a clustering pattern of centrioles in SP bottom before P7, and then re-distributed back to the main SP afterwards. Scale bars: 10 µm. **(B)** An example showing how 3 panels were defined and used for centriole quantification. Scale bars: 10 µm. **(C-D)** Quantification of the number of nuclei and centrioles per square millimeter (nuclei/mm^2 and centriole/mm^2) in the middle and bottom panels of SP from P3 to P14. B: bottom; M: middle. Two-way ANOVA with Bonferroni's multiple comparison test. **(E)** Centriole/Nucleus ratio at SP bottom and SR from P3 to P14. **(F)** Enlarged cilia images of late-born neurons showing that cilia length was increasing, and cilia and centrioles were migrating upward (indicated by cyan arrows) from P7 to P14. Centrioles (white arrows) in the front were followed by cilia axoneme. Scale bars: 10 µm. **(G)** Polar plots of cilia orientation in the upper part of SP from P7 to P14. **(H)** The percentage of south-oriented cilia in the upper part of SP significantly increases from P7 to P14. One-way ANOVA with Bonferroni's multiple comparison test for E & H . **(I)** A schematic diagram depicting principal cell positioning and the reverse migration of centrioles/cilia of late-born neurons in the hippocampal CA1 region.

Fig. 4. Primary cilia directionality in the neocortex indicates a reverse movement of principal neurons during postnatal development. (A-B) Co-immunostaining of AC3, Arl13b and DAPI in Layer

II and V at P3 and P7 from WT mice **(A)** and Arl13b+ mice **(B)**. Scale bars: 5 µm. (**C-D)** Quantification of cilia length in cortical Layer II and V. Primary cilia of early-born neurons are much longer than those of late-born neurons at P3 and P7 in both WT and Arl13b+ mice. Unpaired Student's T-test; *** $p < 0.001$, n = 3 mice, mix sex. **(E-H)** The densities of centrioles and nuclei in the superficial sublayer (Layer II/III) of the neocortex changed from compact and uneven at P3 to sparse and even at P14. The right two panels showing how top and middle sections are defined. Scale bars: 10 µm. **(F)** The ratios of centriole to nucleus (C/N ratio) in both top and bottom of the cortical superficial sublayer at P3 and P14 are all close to 1. The density of nuclei (**G**) and centrioles (**H**) at P3 and P14 are quantified. Two-way ANOVA test with Bonferroni post hoc tests was applied in **(F-H)**. **(I)** The distance from the outer edge of Layer II to the pial surface, which is indicated in **(E)** by red arrows, increases significantly in the first two postnatal weeks. One-way ANOVA test with Bonferroni post hoc tests. (**J-K**) Primary cilia in both the superficial sublayer (Layer II/III) and deep sublayer (Layer V) in the neocortex orientate towards the pial surface. P14 and P40 in WT **(J)** and Arl13b+ **(K)** mice. Scale bars: 10 µm.

Fig. 5. The changes in ratios of neocortical layers during postnatal development are indicative of inward migration. (A) Cortical co-immunofluorescence staining using Satb2 and Ctip2 antibodies. White line indicates whole six layers of the neocortex; red line labels the neocortical superficial sublayer starting from the top edge of Layer V to the pial surface; green line marks Layer VI starting from the bottom edge of layer V to the end of Ctip2 expression. Scale bar: 100 µm. **(B)** The ratio of superficial sublayer to whole 6 layers increases after birth and stabilizes after P20. **(C)** The ratio of deep sublayer V to whole 6 layers decreases postnatally. **(D)** The ratio of Layer VI to whole 6 layers decreases significantly in the first week after birth and stabilize after P20. n=3, mix sex, one-way ANOVA with Bonferroni post hoc tests. **(E)** The distances from Layer VI to the ventricular zone (VZ) decrease over ages. Data of **(E**) were quantified based on red line between the VZ to the edge of Layer VI using Allen Brain Atlas images **(F**). Scale bars: 100 µm.

Fig. 6. CFSE tracing shows the reverse migration of late-born neocortical principal neurons during postnatal development. (A-B) CFSE-tag shows that principal cells undergo a reverse migration during early postnatal stage. **(A)** CFSE dye expression pattern at P1, P3, P9 stays at the injection site, the outermost layer of the superficial sublayer, while at P3, CFSE-labeled superficial sublayer cells appear in the inner part layer, and further inside of the cortex at P9. Scale bar: 100 µm. **(B)** White boxes in **(A)** are zoom in here. Scale bar: 20 µm. **(C-D)** CFSE-labeled migrating cells are ~70% Ctip2-positive cells, indicating that those migrating cells are principal cells. Scale bar: 10 µm. **(E)** Control: little lateral

diffusion was observed at P1 and P9 when CFSE was injected into neocortical inner layers at P 0.5. Scale bars: 100 µm.

Fig. 7. Alterations of primary cilia function affects brain volume and neuronal number. (A) X-ray micro-CT of Ift88 flox/flox Emx1-Cre (Ift88 cKO) mice and controls at P20, scale bar: 1 mm. RSG: granular retrosplenial cortex area. An arrow indicates a gyrification site. **(B)** Thickness of different subregions of neocortex are quantified. One-way ANOVA with Bonferroni post hoc tests. **(C)** Ift88 cKO mice show significantly larger brain size after P5 than controls. One-way ANOVA with Bonferroni post hoc tests. **(D)** Ift88 cKO mice show lower survival rate than controls (n = 20). **(E)** Arl13b flox/flox Emx1-Cre mice (Arl13b cKO) mice show a slightly larger brain at P9, but not at other ages. One-way ANOVA with Bonferroni post hoc tests was used. **(F)** Arl13b+ mice show significantly smaller brain size after P14 than control littermates (n = 4). Two-way ANOVA with Bonferroni post hoc tests. (**G-I**) Altered neuronal composition in neocortical lamina in Ift88 cKO mice. **(G)** Brain sections of Ift88 cKO and control mice at different ages were stained with Satb2 and Ctip2. Representative images of Layer V are shown. (**H**) Ift88 cKO mice had more Satb2-positive neurons (relative to nucleus counts) in Layer V from P5 to adulthood, but not before at P0 and P3. (**I**) There are no significant differences in Ctip2-positive neurons in Layer V between Ift88 cKO and control mice from P0 to adulthood.

Fig. 8. Selective ablation of primary cilia in the forebrain leads to gyrification in the retrosplenial cortex that occurs postnatally and is formed by reverse migration. (A-B) Ift88 cKO mice starts to show a very shallow sulcus at E18.5 in the retrosplenial cortex, and the depth of sulcus increases drastically from P0 to P9, and then stabilize after P9. Scale bar: 100 µm. **(C)** Statistical data: the distances from the midline to the edge of the superficial sublayer or gyrification site. Not only the degree of gyrification of cKO mice, but also the distance from the midline to the edge of the superficial sublayer in controls mice increase with age. **(D)** Immunostaining using Ctip2 from P0 to P20 in the retrosplenial cortex of WT mice. White line represents the perpendicular distance from the brain midline to the edge of deep sublayer site in the retrosplenial cortex (marked by Ctip2), which are quantified in **(E)**. Scale bar: 100 µm.

Fig. 9. Selective disruptions of primary cilia function in the forebrain lead to altered CA1 lamination. (**A**) Co-immunofluorescence staining using Satb2 (red), Ctip2 (green) and DAPI (bule) on P5 control and Ift88 flox/flox Emx1-Cre (Ift88 cKO mice). Ift88 cKO mice show significant difference in the distal CA1 at P5. Scale bar: 100 µm. (**B**) CA1 SP thickness naturally decreases with age in controls (top), Ift88 cKO

mice exhibit delayed lamina condensation (bottom) and misplacement of cells in the 10 µm thickness CA1 SP. Scale bar: 10 µm. (**C**) Quantification of CA1 thickness from different ages. n = 3, total 9 regions total were quantified, Two-way ANOVA with Bonferroni post hoc tests. **(D)** Thickness quantification of the distal and proximal in CA1 SP at P5. n = 3, total 9 regions total were quantified. (**E**) Cilia are ablated in CA1 regions of Ift88 cKO mice and shorten in Arl13b cKO mice. Scale bar: 10 µm. (**F**) Disruption of cilia function causes loosened distribution of principal neurons in CA1 SP (indicated by white arrows). Scale bars: 10 µm.

Fig. 10. Disruption of primary cilia function causes neuronal misplacement in DG. (**A**) representative images of AC3-labeled primary cilia in the granular cell layer. Centrioles were marked by Centrin2-GFP. Right panels are enlarged. **(B)** Polar plot of primary cilia orientation. Primary cilia in the outer part of the granular cell layer at P14 are oppositely orientated. Scale bar: 10 µm. (**C**) Arl13b-labeled primary cilia are more prevalent at P9, while AC3-labled primary cilia are more abundantly expressed at P20 in the granular cell layer. Scale bar: 10 µm. (**D-G**) Cilia alterations led to misplaced neurons in DG. (**D**) Primary cilia are ablated in Ift88 cKO mice and shortened in Arl13b cKO mice. Scale bar: 10 µm. (**E**) Ift88 cKO and Arl13b cKO mice lose the compactness of the granular cell layer. Both coronal and sagittal sections show similar patterns. Scale bar: 100 µm. (**F**) A diagram depicting the quantification method of misplaced neurons in the outer molecular layer of DG. (**G**) Quantification results of misplaced neurons in DG of coronal sections (left) and sagittal sections (right). Two-way ANOVA with Bonferroni post hoc tests were used for statistical analysis.

Supplemental Figures:

Fig. S1. Allen Brain Atlas *in situ* hybridization staining of Ndst4 over ages, Col11a1 and Htr1a at P56 in mouse hippocampal CA1. (A) The thickness of the CA1 SP continues to decrease with age. The mRNA of Ndst4 (a deep sublayer marker gene) was mostly expressed in the deep sublayer of CA1 SP, but the distribution was dynamic as age. M: month. **(B)** Col11a1 mRNA was mostly expressed in the deep sublayer, but also slightly dispersed to the superficial sublayer at P56. **(C)** Htr1a mRNA was mostly present in the superficial sublayer and covers most, but not all area of SP at P56. Images credit: Allen Institute for Brain Science.

Fig. S2. Strong regulation of CA1 neuronal cilia length by Arl13b. (A-B) Arl13b+ mice in C57Bl/6J background had much longer neuronal primary cilia than WT mice in the hippocampal subregions (CA1, CA3 and DG) in adults. Notably, CA1 region had the longest primary cilia and the effect of Arl13b on

promoting cilia length is very strong. Compared with WT mice, the average CA1 cilia length increase by over 60% in Arl13b+ mice. **(C-D)** Compared to hippocampal regions, primary cilia length is not strongly changed in other brain regions such as neocortex and amygdale. Immunostaining of neuronal primary cilia in WT controls and Arl13b overexpression transgenic (Arl13b+) mice. Unpaired Student's T-test was applied in (**B** and **D**). Scale bar: 10 µm. Data were collected from at least 3 young adult mice for each genotype. Mix sex.

Fig. S3. Ciliation roughly coincides with neuronal maturation in the CA1 SP. (A) Early-born neurons in the deep sublayer protruded cilia earlier than neurons in the superficial sublayers at P3 in Arl13b+ mice, and those early-protruding cilia point towards the north. WT CA1 also had few north-pointing cilia. **(B)** NeuN expression was first detected in deep-sublayer of SP at P1, more at P5, then extended to superficial-layer neurons at P7. At P14, both deep- and superficial-layer neurons had abundant NeuN expression. Scale bars: 10 µm. **(C-D)** Allen Brain Atlas in situ hybridization (ISH) results of Shank3 and Homer1, two synaptic makers of excitatory neurons, in hippocampal CA1 at P4 and P14. At P4, Shank3 and Homer1 are only expressed in the deep sublayer of SP and Layer V (deep sublayer) of the neocortex. At P14, ISH signals of two genes are presented in most area of SP and the six layers in the neocortex. Scale bars: 100 µm.

Fig. S4. The primary cilia of early- and late-born neurons in the ventral hippocampal CA1 region clearly display opposite directionality. Representative images of primary cilia in the ventral CA1 regions at P9. Top Left panels are enlarged images at P9. Data from WT brain sections were strained with AC3 and Arl13b antibodies. Arl13b+ primary cilia and centrioles were marked by Arl13b-mCherry and Centrin2-GFP, respectively. Bottom panels are polar plots of primary cilia orientations of WT and Arl13b+ at P9 and P40. Arrows indicate the changes of SO-pointing cilia orientations from P9 to P40.

Fig. S5. CA3 neurons mature and protrude neuronal primary cilia earlier than CA1 neurons. (**A-C**) The hippocampal CA3 region of WT and Arl13b+ mice abundantly express primary cilia at P5 and P7, earlier than CA1 (see Fig. 1-2). Scale bars: 10 µm. (**D**) CA3 pyramidal neurons mature earlier than CA1 neurons. At P4, CamK2a and PSD-95, two postsynaptic marker proteins, are highly and widely expressed throughout the CA3. In contrast, their expression is only restricted to the deep sublayer of CA1, not present in the superficial sublayer at P4. Scale bars: 100 µm. ISH images were adopted from the Allen Brain Atlas Developing Mouse Brain. Images credit: Allen Institute for Brain Science. (**E**) Primary cilia directionality in the CA3 region is different from that of CA1. Confocal imaging was collected from Arl13b+ mice.

Fig. S6. (A-B) Only principal neurons in laminated brain regions exhibit specific cilia directionality. **(A)** Immunostaining of cilia in different brain regions including subiculum, thalamus, hypothalamus, and neocortex. Scale bar: 10 µm. **(B)** A diagram summarizing the orientation of neuronal primary cilia in multiple brain subregions. **(C-G)** Primary cilia of interneurons and astrocytes do not display specific directionality. **(C)** Interneurons' primary cilia do not point to specific direction. Straining using Ift88 flox/flox Camk2a-Cre P20 sections shows remaining primary cilia of interneurons in the hippocampal CA1 and neighboring neocortex. Because AC3 is a marker for neuronal primary cilia and the Camk2a-Cre strain selectively express Cre in forebrain principal neurons, primary cilia marked by AC3 in Ift88 flox/flox Camk2a-Cre belong to interneurons. **(D)** Astrocytic primary cilia (denotes by white arrows) in the hippocampus do not exhibit specific directionality. (**E**) Astrocytic primary cilia in the neocortex do not exhibit specific directionality. Two representative images are shown. White arrows denote astrocyte cilia, which display irregular pointing. Green arrows denote neuronal primary cilia, which point to the pia. (**F-G**) Polar plots of astrocytic primary cilia orientation in the hippocampus (**F**) and neocortex (**G**). D-G data were collected from Arl13b-mCherry brain sections that were stained by Arl13b and GFAP antibodies.

Fig. S7. Subiculum and postsubiculum exhibit a reverse movement for lamina formation during postnatal development. **(A)** Ctip2 ISH staining from E18.5, P4 and P14 of mouse sagittal sections. Images in the top are partially enlarged in the bottom. Bule arrows denote the curvature between the postsubiculum that emerge at P4 and becomes remarkable at P14. Red arrows point to the demarcation between CA1 and subiculum, which becomes more obvious with age. **(B)** Similar pattern changes in the CA1, subiculum, postsubiculum and neocortex are observed in Etv1 ISH staining. Staining using other markers show similar departmental pattern. VZ: the ventricular and subventricular zone, Sub: subiculum, POST: postsubiculum. ISH Data were adopted from Allen Brain Atlas.

Fig. S8. Primary cilia are selectively ablated and shortened in the forebrain in Ift88 cKO mice and Arl13b cKO mice, respectively. (**A-C**) Primary cilia were deleted in the hippocampus and neocortex of Ift88 cKO mice at P9 and P20. RSG: granular retrosplenial cortex area, DG: dentate gyrus. **(D-F)** Primary cilia were present in other brain regions of Ift88 cKOs including the 3rd ventricle, and the kidneys. Scale bars: 10 µm. (**G-I**) Primary cilia were selectively shortened in the forebrain of Arl13b cKO mice. **(G)** Primary cilia were shortened in the neocortex in Arl13 cKO mice. Layer II/III: neocortex Layer II and III.

RSG: granular retrosplenial cortex area. **(H-I)** Primary cilia were normal in other brain regions such as hypothalamus and 3rd ventricle in KO mice. Scale bars: 10 µm, all images were collected from P9 mice.

Fig. S9. A working model of postnatal principal cell positioning. A slow reverse migration is required for refining inside-out laminae spanning from the neocortex to the hippocampal CA1. In the neocortex or sparse layers, both early- and late-born neurons reverse. In the hippocampal CA1 region or other inside-out layers, late-born neurons reverse, whereas early-born neurons do not. White and blue arrows indicate the direction of radial migration of principal cells and postnatal reverse migration, respectively. Deep: deep sublayer; Super.: superficial sublayer. VZ: the ventricular zone. The early-born and late-born neurons in the CA3 are not as well separated as in the CA1. Additionally, DG lamina is formed by outside-in migration pattern. Thus, CA3 and DG may have distinct positioning mechanisms and thereby do not fit to this model.

Tables:

Regions	CA1 -deep	CA1 -super.	Cortex -deep	Cortex -super.	CA3 -deep	CA3 -super.	DG-out¶	DG-in¶
Ciliation Time (WT)	P3-P7	P9-P10	P3-P7	P7-P10	P3-P7	P3-P7	P3-P7	After P7
Ciliation Time (Arl13B+)	P0-P7	P7-P10	P0-P7	P7-P10	P0-P7	P0-P7	P0-P7	After P7
Cilia Orientation	Point to SO	Point to SR	Point to pial surface	Point to pial surface	Largely† point to SO	Largely† point to SR	TBD	To outer layer?
Cilia Length (WT)	<1 µm, P7	<1 µm, P7	3.3±0.1 µm, P7	1.0±0.0 µm, P7	5.6±0.1 µm, Adult		2.3±0.0 µm, Adult	
	7.0±0.1 µm, Adult		5.6±0.1µm, Adult	5.0±0.0 µm, Adult				
Cilia Length (Arl13B+)	1.5±0.0 µm, P3	1.0±0.0 µm, P3	1.9±0.1 µm P3	0.7±0.0 µm P3	8.2±0.1 µm, Adult		3.1 ± 0.0 µm, Adult	
	4.5±0.1 µm, P7	2.8±0.1 µm, P7	4.5±0.1 µm P7	2.1±0.1 µm P7				
	11.7±0.1 µm, Adult		6.3±0.1 µm, Adult	5.3±0.0 µm, Adult				
Reverse Migration	No	Yes	Yes	Yes	TBD			
NeuN# Expression	P3-P5	P7-P14	P0-P1	P5	P3-P5	P3-P5‡	P5-P7	P7-P10
Camk2a* Expression	~P4	P4-P14	~P4	P4-P14	~E18.5-P4	~E18.5-P4	P4	After P4
Shank3* Expression	~P4		~P4		~E18.5-P4	TBD		
Homer 1* Expression	~P4		~P4		~P4-P14	~P4-P14		
PSD-95* Expression	~P4 or earlier		~P4 or earlier		~E18.5-P4	~E18.5-P4		
Synapsin 1* Expression	~P4		~P4		~ E18.5-P4	~E18.5-P4		
Syntaxin1* Expression	~P4		~P4 or earlier		~ E18.5-P4	~ E18.5-P4	Not expressed	Not expressed

TBD: to be determined. Super., superficial sublayer. P: postnatal; E: embryonic. Adult: 2–4 months old. ¶ Dentate gyrus outer granular layer and inner granular layer. † CA3 deep-superficial distinction in ciliation and neuronal maturation is not as obvious as CA1. ? Require further verification. ‡ CA3 pyramidal neurons mature several days earlier than CA1 neurons. # Based on our immunostaining data using anti-NeuN antibody. ƒ Outmost superficial layer in the neocortex * Based on ISH data from the Allen Brain Atlas Developing Mouse Brain.

Table 1. Features of neuronal primary cilia and neuronal maturation in subregions of the hippocampus and neocortex.

Brain Regions or Cell Types	Primary Cilia Directionality	Cell Density in Lamina
DG	Opposite	Compact
CA1	Opposite	Compact
CA3	Opposite (?)	Compact
Olfactory Tubercle	Opposite	Compact
Piriform Cortex (Layer II)	Opposite	Compact
Piriform Cortex (Layer III)	Same, to the pia	Loose
Neocortex	Same, point towards the pia	Loose
Entorhinal Cortex	Same, to the pia	Loose
Subiculum	Same, to the pia	Loose
Postsubiculum	Same, to the pia	Loose
CA1 Interneurons	Irregular	Not layered
CA1 Astrocytes	Irregular	Not layered
Cortex Astrocytes	Irregular	Not layered
Thalamus	Irregular	Not layered
Hypothalamus	Irregular	Not layered
Amygdala	Irregular	Not layered
Striatum	Irregular	Not layered

Table 2. Primary cilia directionality in different brain regions or cell types, in connection with cell density and lamination. Primary cilia orientation may change with age, but the best timing to measure cilia directionality is P14-P20, when neurons complete the postnatal positioning step.

Cortical Regions		Speed (μm/hr)	Estimation Methods	Impacts
CA1-SP	Deep	No	Centriole position unchanged and cilia orientate toward north	SP gradually becomes compact and narrow
	Super.	0.1-0.2	Centriole movement and SP lamina thickness change	
CA3-SP	Deep	Unclear	Early- and late-born neurons highly mingled, unable to estimate reverse speed	Deep-superficial lamination in CA3 SP different from CA1 SP
	Super.			
Subiculum*		0.2-0.3	Lamina upward shift and expansion, cilia orientation	Generate a sparse lamina distinct from CA1
Postsubiculum*		0.4-0.6	Laminae backward shift and expansion, cilia orientation	Form sparse laminae with inward curvature
Neocortex	Super.	1-3	Neuron tracing by CFSE dye	Laminae become sparse and even;
	Deep*	0.5-2	Layer VI to VZ distance change	
Retrosplenial cortex (WT)		0.3-0.6	Postnatal changes in Layer I-VI	Layer I expand and Layer II-VI principal neurons move inward
Retrosplenial cortex (Ift88 lox/lox Emx1-cre mice)		0.8-1.2	Postnatal changes in gyrification	Develop gyrification
Claustrum[§]		*5.2±0.6*	*Oshima et al., 2023 J. Neurosci[100].*	Form claustrum
Developing Neocortex *"Multipolar migration"*		*1.6-6.4*	*Tabata et al., 2003 J. Neurosci[89].*	Outward migration to form the outer layer
Developing Neocortex *"Radial migration"*		*9-12 or 38.6±4.7*	*Tabata et al., 2003 J. Neurosci[89]. Borrell et al., 2006 Cerebral Cortex[101].*	
No: No reverse migration. * Estimation based on my own imaging data and Allen Brain Atlas. VZ: the ventricular zone. [§] This reverse migration occurs during the embryonic stage and has a higher speed.				

Table 3. Features of reverse migration and its impacts on lamina configurations in the cerebral cortex. Note that the speed of reverse migration is a very rough estimation, rigorous assays are needed to precisely determine the speed.

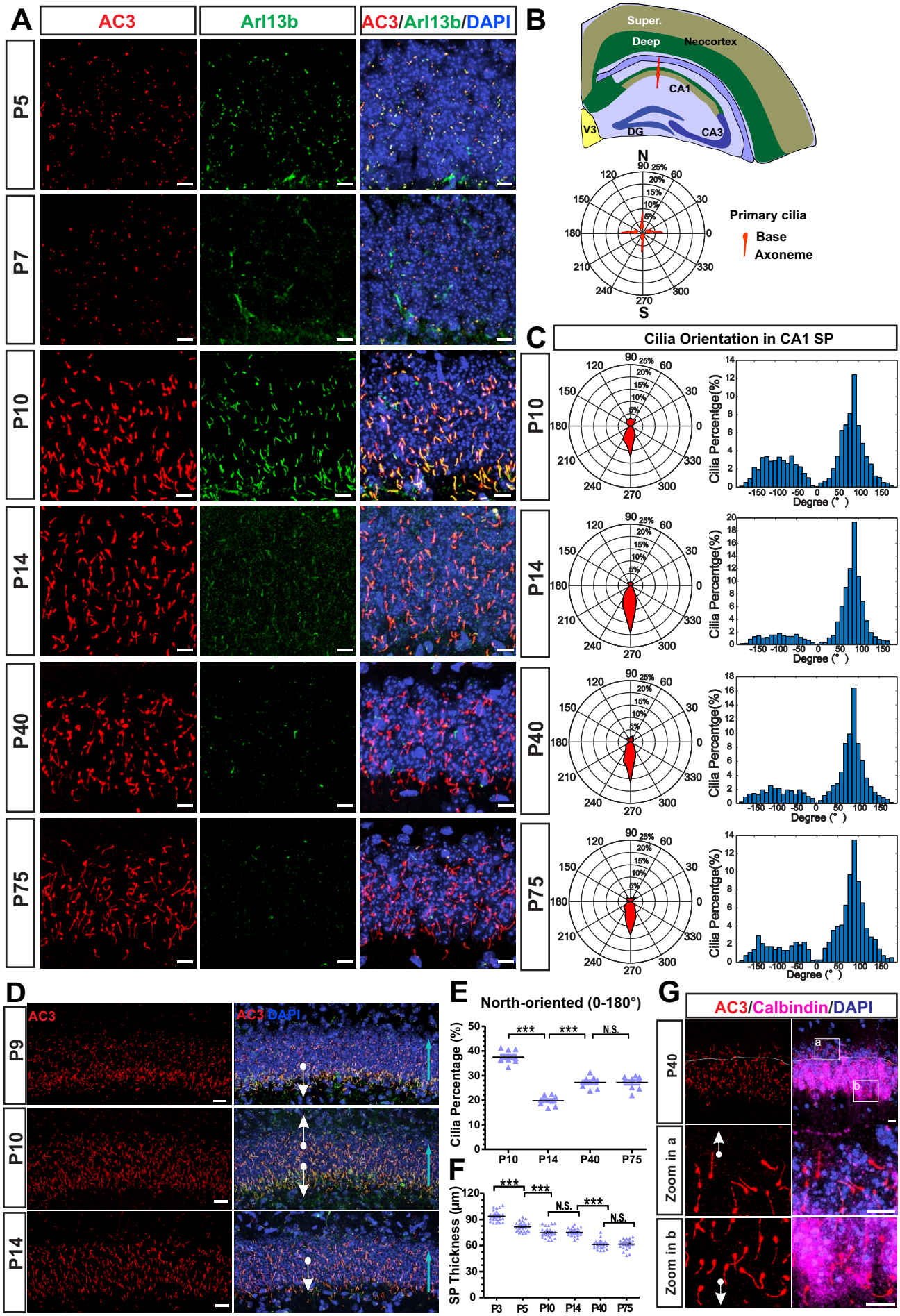
A
AC3
Arl13b
AC3/Arl13b/DAPI
P5
P7
P10
P14
P40
P75
B
Super.
Deep
Neocortex
CA1
V3
DG
CA3
N
S
Primary cilia
Base
Axoneme
C
Cilia Orientation in CA1 SP
Cilia Percentge(%)
Degree (°)
D
AC3
AC3 DAPI
P9
P10
P14
E
North-oriented (0-180°)
Cilia Percentage (%)
P10
P14
P40
P75
N.S.
F
SP Thickness (μm)
P3
P5
P10
P14
P40
P75
G
AC3/Calbindin/DAPI
P40
Zoom in a
Zoom in b

Fig. 1

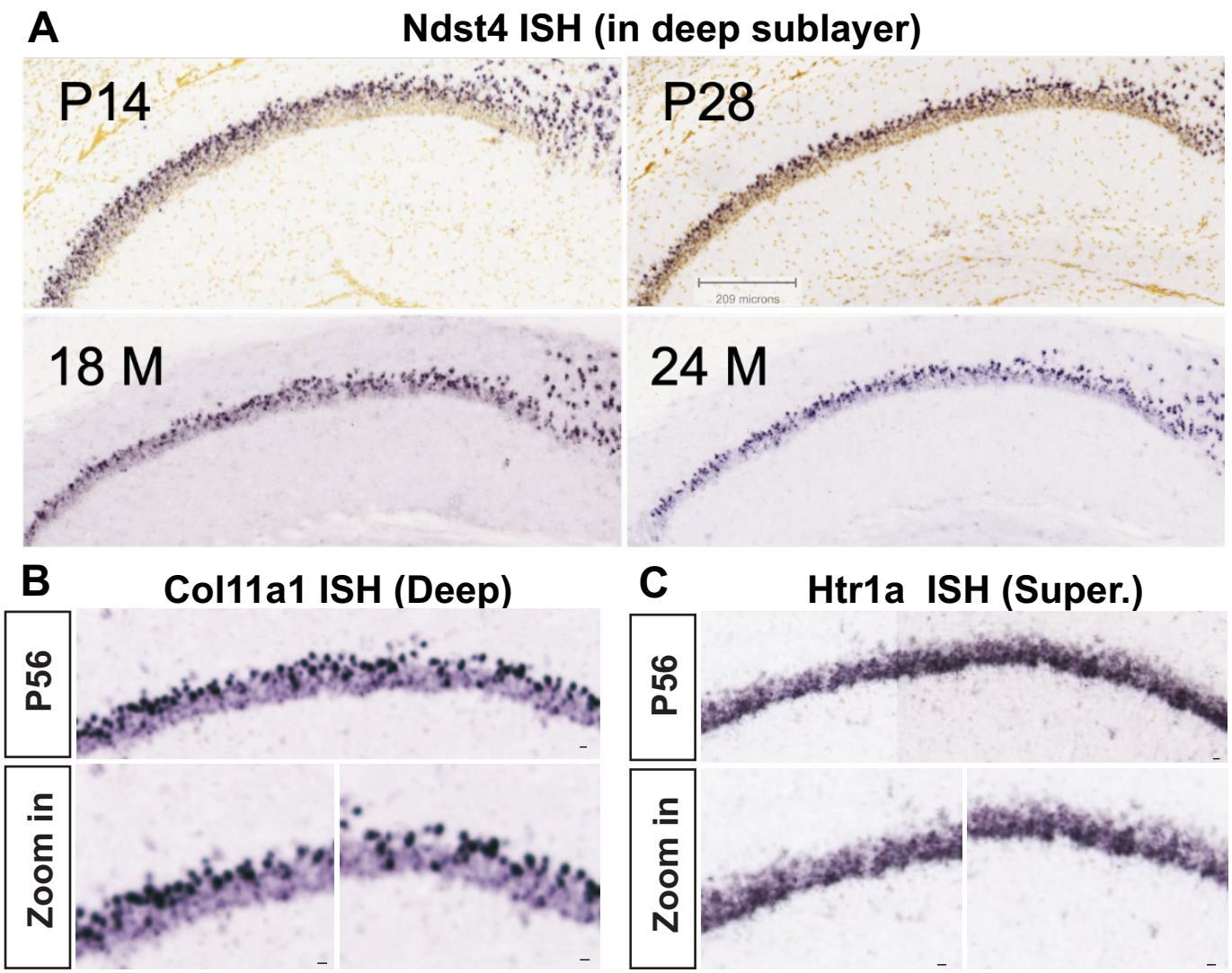
A
Ndst4 ISH (in deep sublayer)
P14
P28
209 microns
18 M
24 M
B
Col11a1 ISH (Deep)
P56
Zoom in
C
Htr1a ISH (Super.)
P56
Zoom in

Fig. S1

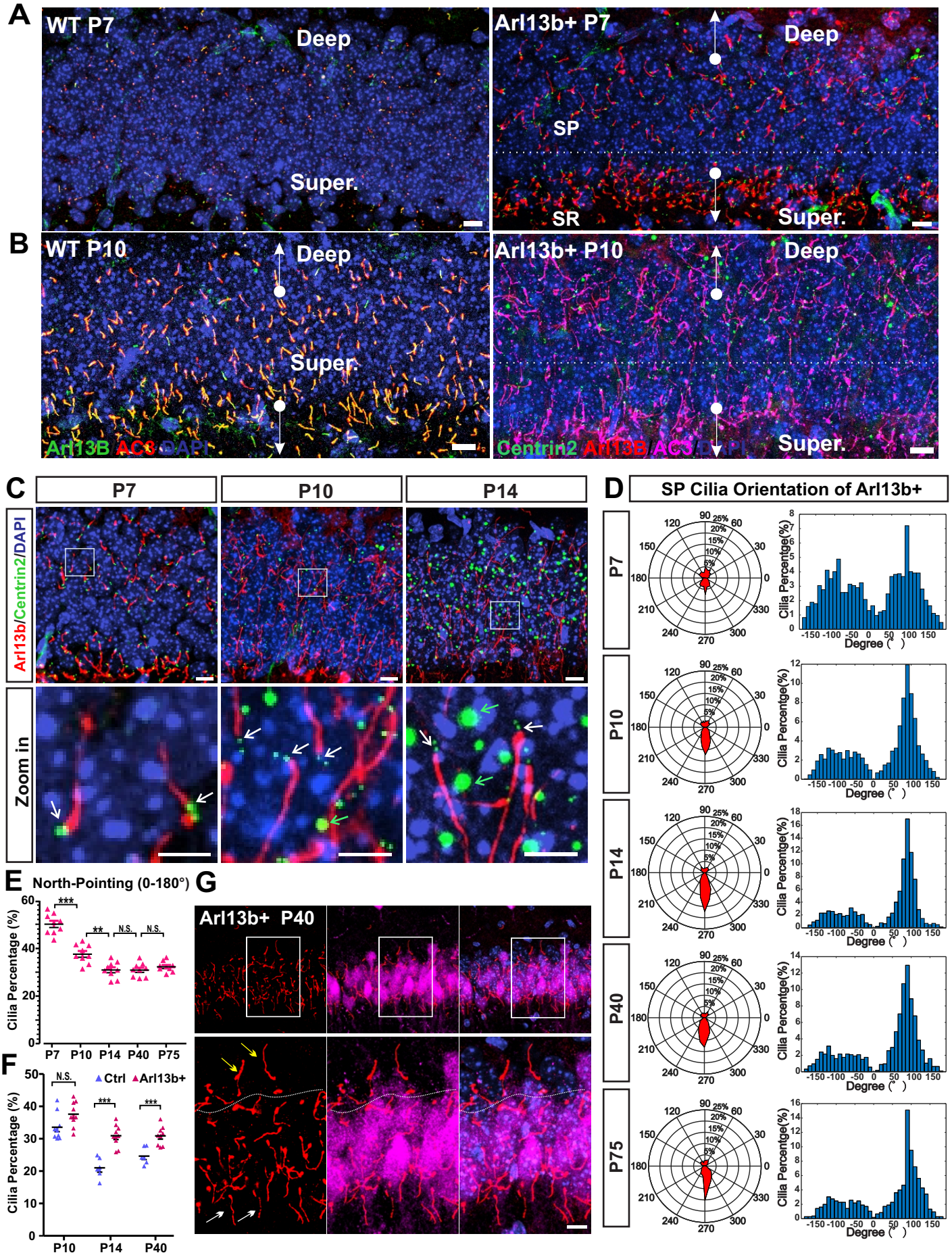
A
WT P7
Deep
Super.
Arl13b+ P7
Deep
SP
SR
Super.
B
WT P10
Deep
Super.
Arl13B AC3 DAPI
Arl13b+ P10
Deep
Super.
Centrin2 Arl13B AC3 DAPI
C
P7
P10
P14
Arl13b/Centrin2/DAPI
Zoom in
D
SP Cilia Orientation of Arl13b+
P7
P10
P14
P40
P75
Cilia Percentge(%)
Degree (°)
E
North-Pointing (0-180°)
Cilia Percentage (%)
P7 P10 P14 P40 P75
***
**
N.S.
N.S.
F
Ctrl
Arl13b+
Cilia Percentage (%)
P10 P14 P40
N.S.
***
***
G
Arl13b+ P40

Fig. 2

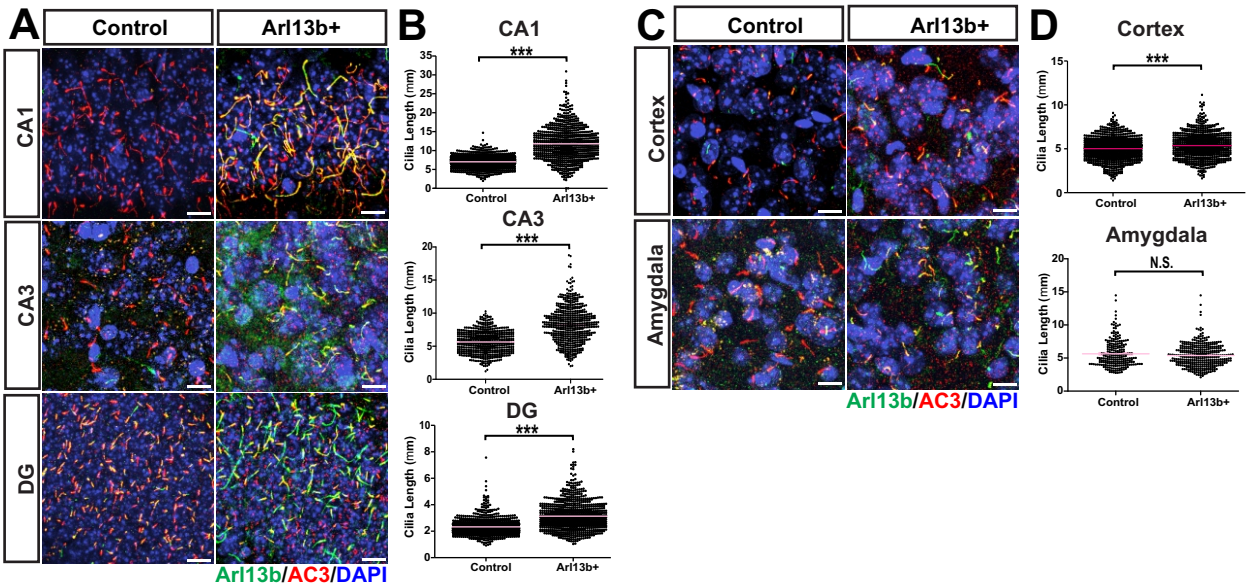
A
Control
Arl13b+
CA1
CA3
DG
Arl13b/AC3/DAPI
B
CA1
CA3
DG
Cilia Length (mm)
Control
Arl13b+
***
C
Control
Arl13b+
Cortex
Amygdala
Arl13b/AC3/DAPI
D
Cortex
Amygdala
N.S.

Fig.S2

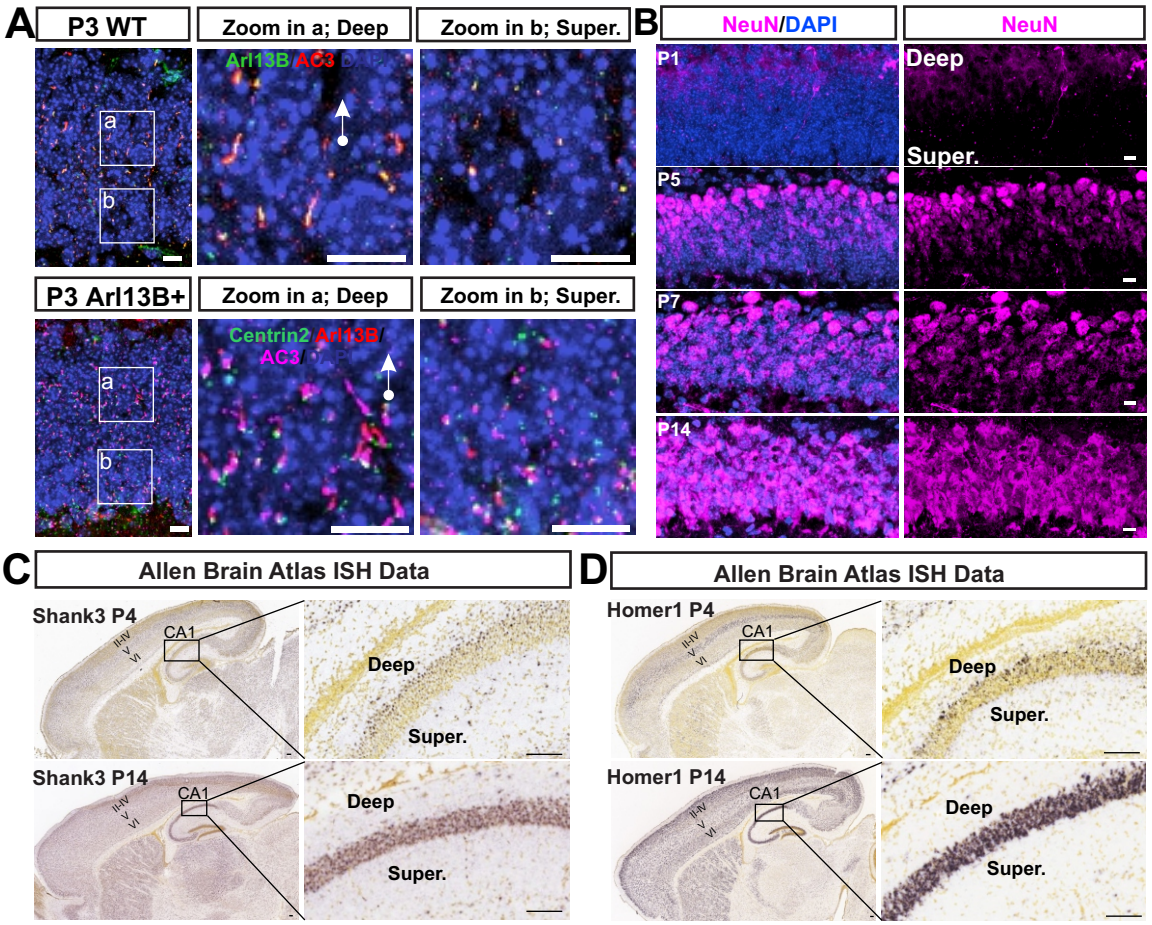
A
P3 WT
Zoom in a; Deep
Zoom in b; Super.
Arl13B/AC3/DAPI
a
b
P3 Arl13B+
Zoom in a; Deep
Zoom in b; Super.
Centrin2/Arl13B/
AC3/DAPI
B
NeuN/DAPI
NeuN
P1
P5
P7
P14
Deep
Super.
C
Allen Brain Atlas ISH Data
Shank3 P4
Shank3 P14
CA1
II-IV
V
VI
Deep
Super.
D
Allen Brain Atlas ISH Data
Homer1 P4
Homer1 P14
CA1
II-IV
V
VI
Deep
Super.

Fig.S3

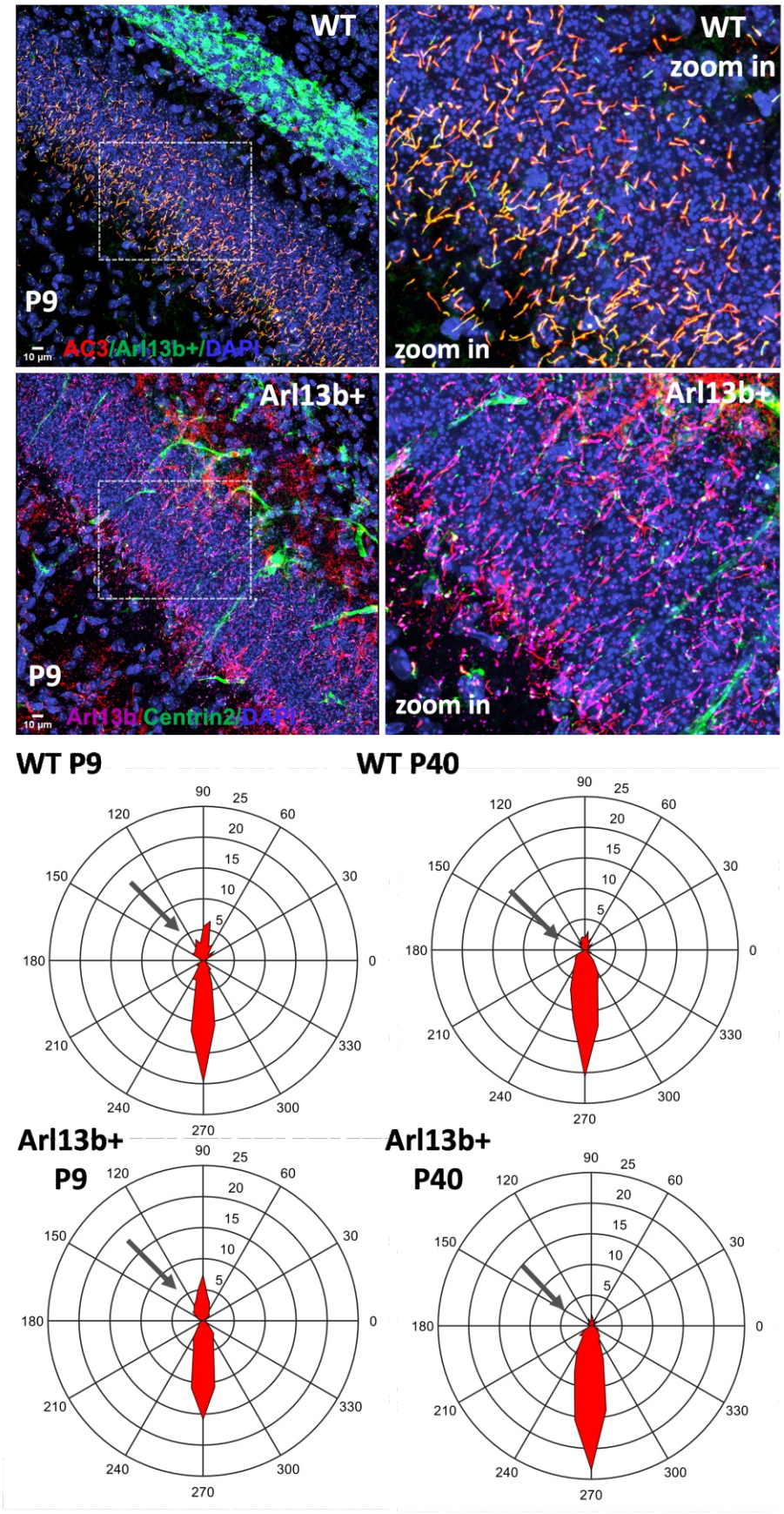
WT
P9
10 µm
AC3/Arl13b+/DAPI
WT
zoom in
zoom in
Arl13b+
P9
10 µm
Arl13b/Centrin2/DAPI
Arl13b+
zoom in
WT P9
WT P40
Arl13b+
P9
Arl13b+
P40
90
25
60
30
0
330
300
270
240
210
180
150
120
20
15
10
5

Fig.S4

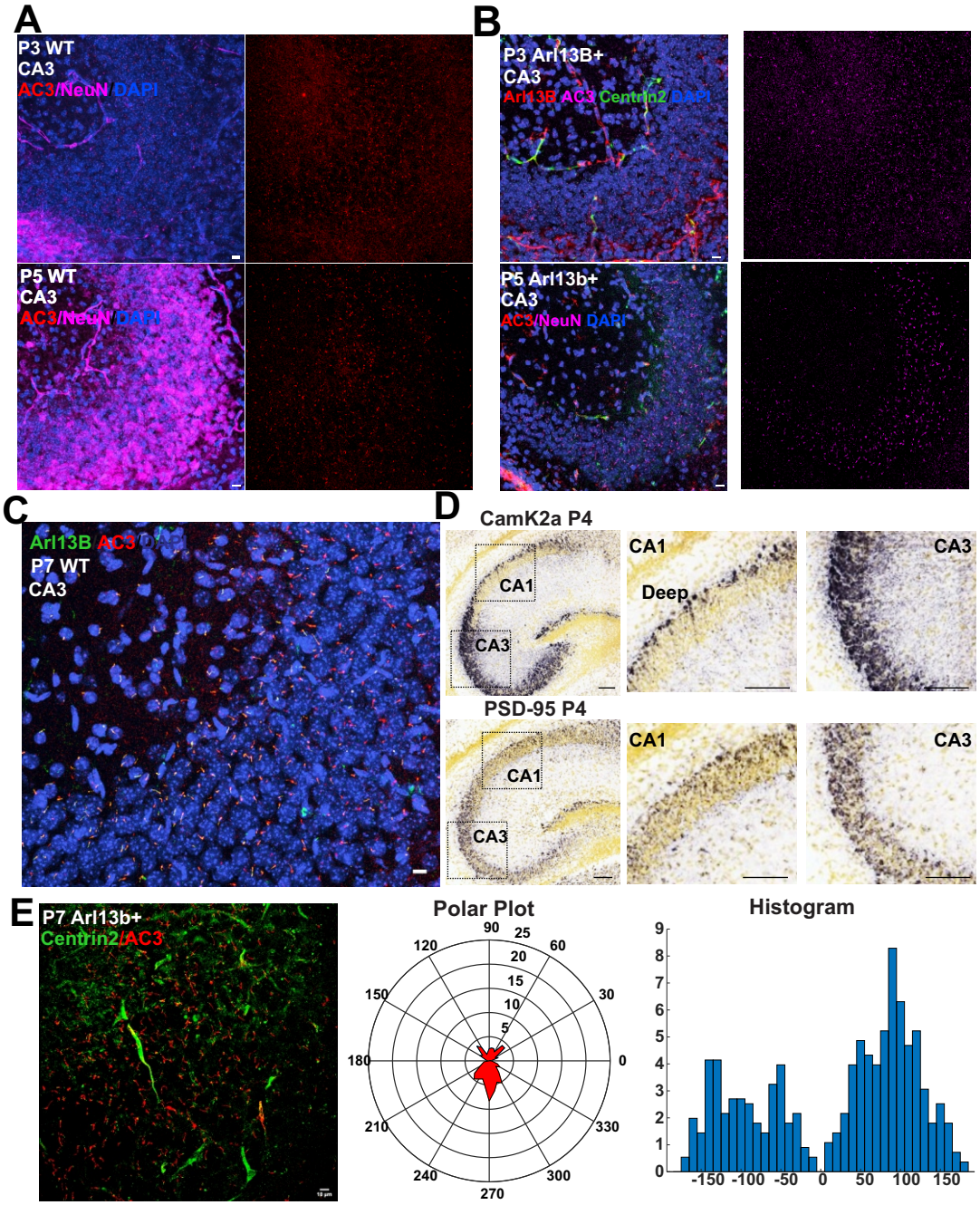
A
P3 WT
CA3
AC3/NeuN/DAPI
P5 WT
CA3
AC3/NeuN/DAPI
B
P3 Arl13B+
CA3
Arl13B AC3 Centrin2/DAPI
P5 Arl13b+
CA3
AC3/NeuN DAPI
C
Arl13B AC3 DAPI
P7 WT
CA3
D
CamK2a P4
CA1
CA3
Deep
PSD-95 P4
CA1
CA3
E
P7 Arl13b+
Centrin2/AC3
Polar Plot
Histogram

Fig.S5

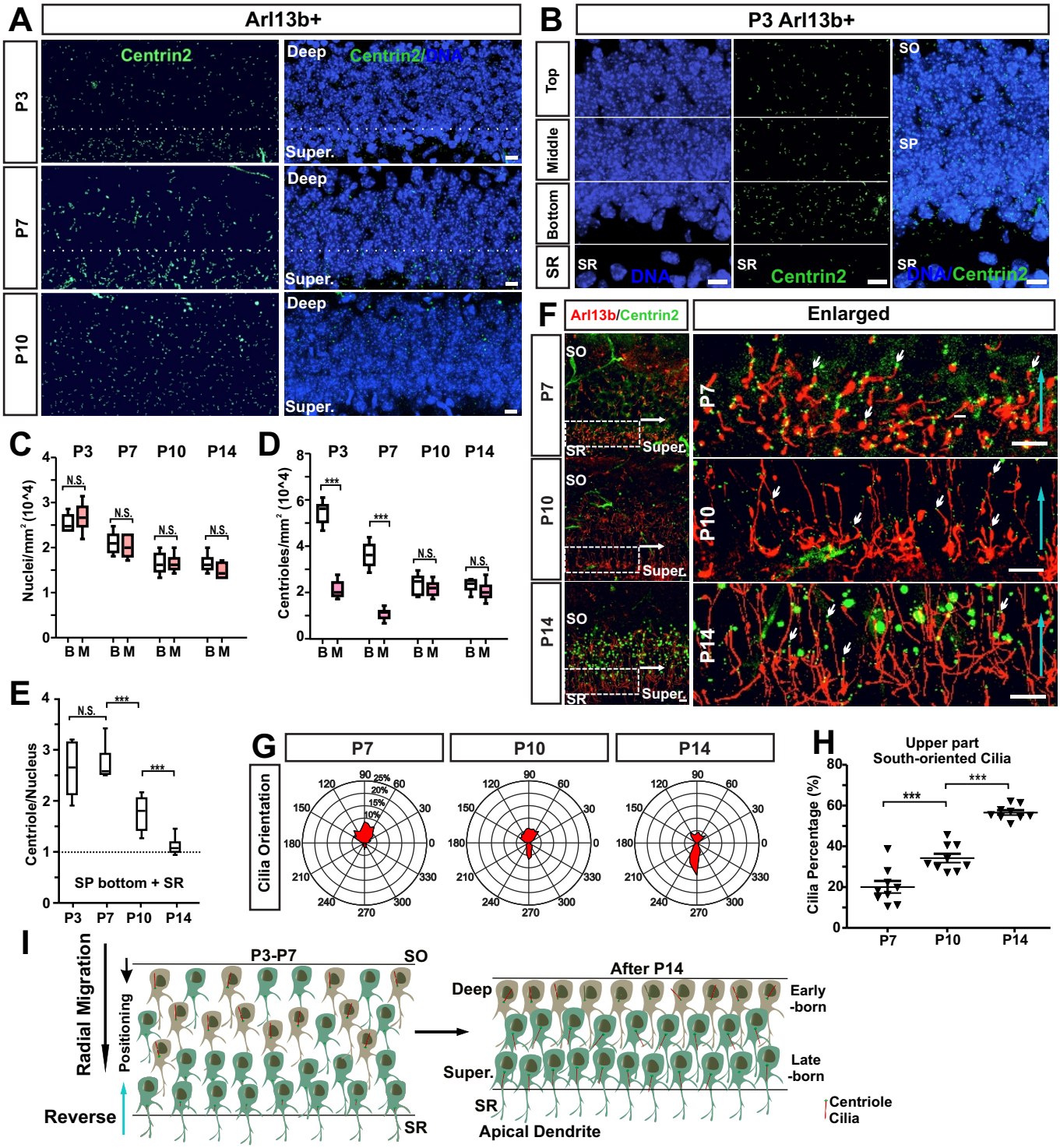
A
Arl13b+
P3
P7
P10
Centrin2
Centrin2/DNA
Deep
Super.
B
P3 Arl13b+
Top
Middle
Bottom
SR
SO
SP
DNA
Centrin2
DNA/Centrin2
C
P3 P7 P10 P14
Nuclei/mm² (10^4)
N.S.
B M
D
Centrioles/mm² (10^4)
***
E
Centriole/Nucleus
SP bottom + SR
F
Arl13b/Centrin2
Enlarged
G
Cilia Orientation
H
Upper part
South-oriented Cilia
Cilia Percentage (%)
I
Radial Migration
Positioning
Reverse
P3-P7
After P14
Deep
Super.
Early -born
Late -born
Centriole
Cilia
Apical Dendrite

Fig. 3

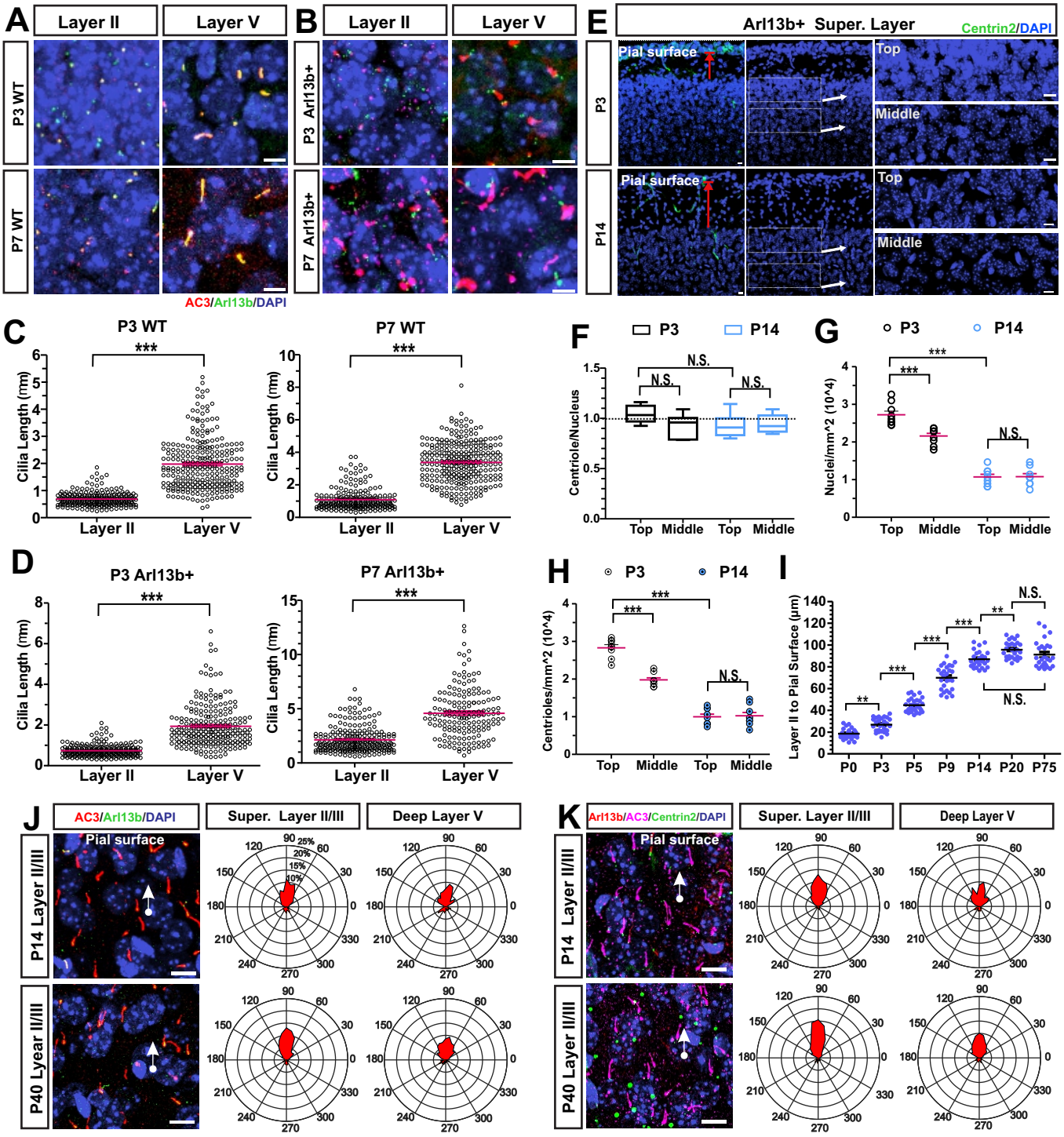
A
Layer II
Layer V
P3 WT
P7 WT
AC3/Arl13b/DAPI
B
P3 Arl13b+
P7 Arl13b+
E
Arl13b+ Super. Layer
Centrin2/DAPI
Pial surface
Top
Middle
P3
P14
C
P3 WT
P7 WT
Cilia Length (mm)
Layer II
Layer V
D
P3 Arl13b+
P7 Arl13b+
F
P3
P14
Centriole/Nucleus
N.S.
G
Nuclei/mm^2 (10^4)
H
Centrioles/mm^2 (10^4)
I
Layer II to Pial Surface (µm)
P0
P3
P5
P9
P14
P20
P75
J
AC3/Arl13b/DAPI
Super. Layer II/III
Deep Layer V
P14 Layer II/III
P40 Lyear II/III
K
Arl13b/AC3/Centrin2/DAPI
P40 Layer II/III

Fig. 4

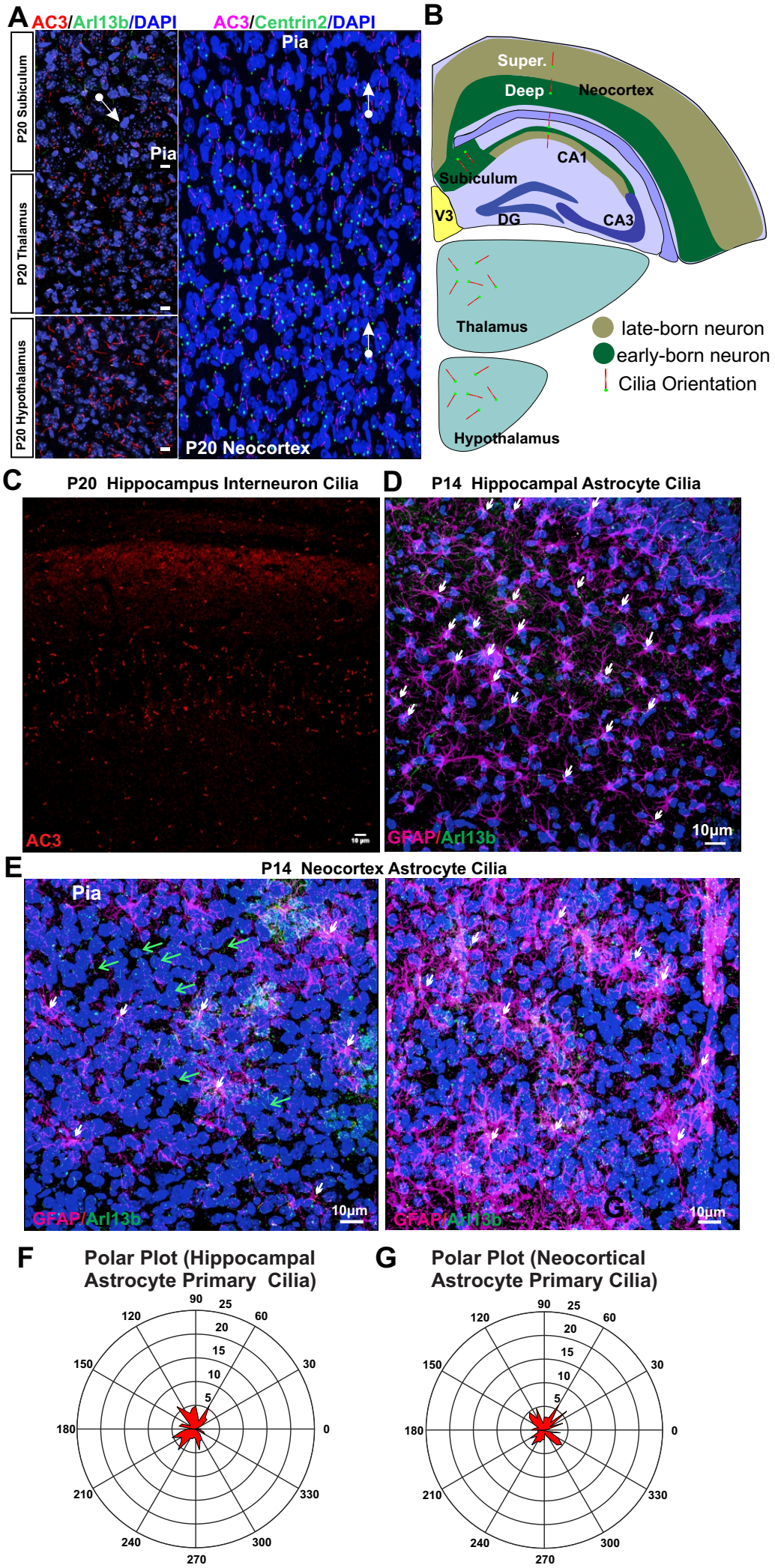
A
AC3/Arl13b/DAPI
AC3/Centrin2/DAPI
P20 Subiculum
P20 Thalamus
P20 Hypothalamus
Pia
Pia
P20 Neocortex
B
Super.
Deep
Neocortex
CA1
Subiculum
V3
DG
CA3
Thalamus
Hypothalamus
late-born neuron
early-born neuron
Cilia Orientation
C
P20 Hippocampus Interneuron Cilia
AC3
D
P14 Hippocampal Astrocyte Cilia
GFAP/Arl13b
10μm
E
P14 Neocortex Astrocyte Cilia
Pia
GFAP/Arl13b
10μm
GFAP/Arl13b
10μm
F
Polar Plot (Hippocampal Astrocyte Primary Cilia)
G
Polar Plot (Neocortical Astrocyte Primary Cilia)
90
25
20
15
10
5
120
60
150
30
180
0
210
330
240
300
270

Fig. S6

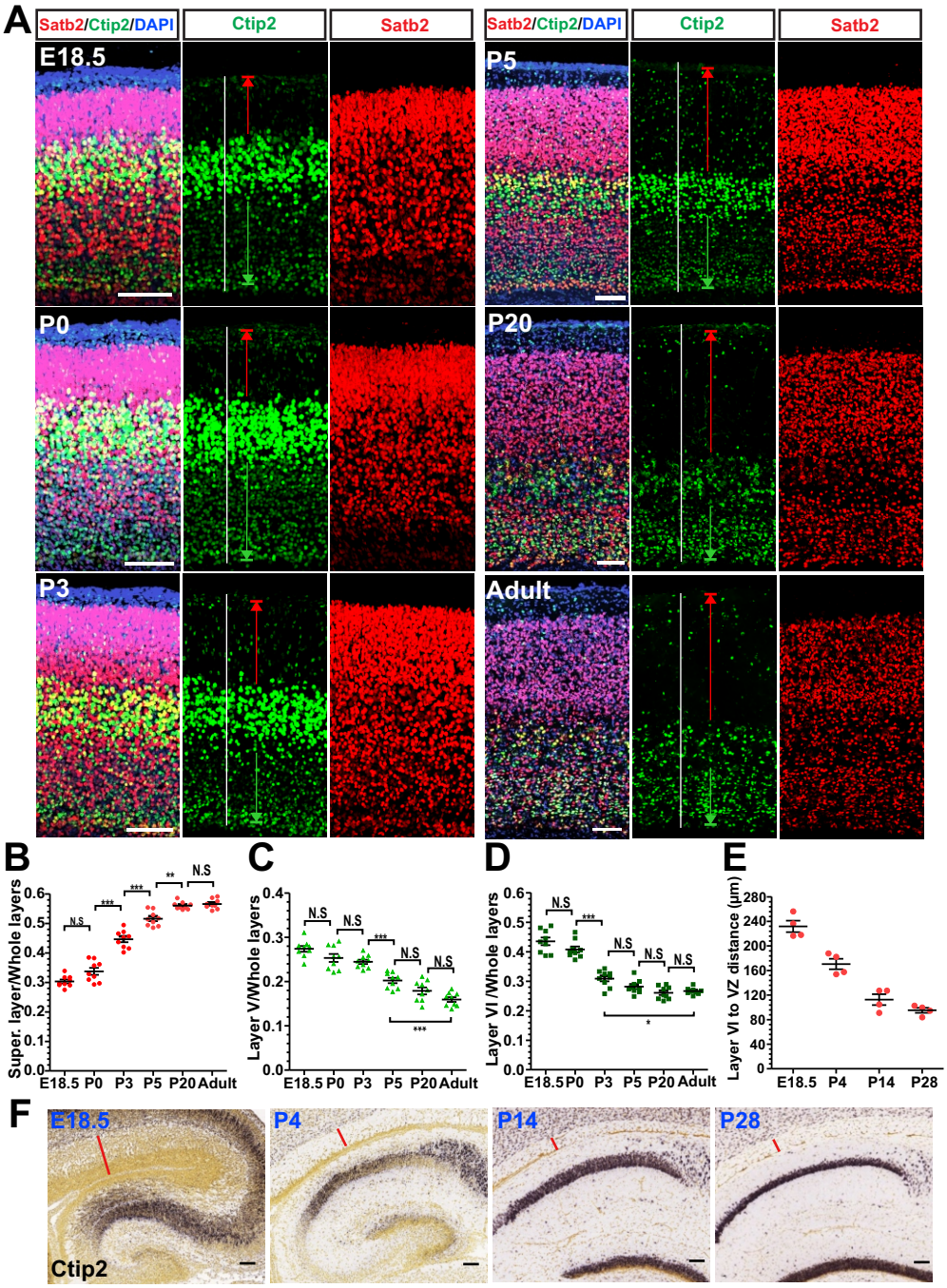
A
Satb2/Ctip2/DAPI
Ctip2
Satb2
E18.5
P5
P0
P20
P3
Adult
B
Super. layer/Whole layers
N.S
***
**
E18.5 P0 P3 P5 P20 Adult
C
Layer V/Whole layers
N.S
***
E18.5 P0 P3 P5 P20 Adult
D
Layer VI /Whole layers
N.S
***
*
E18.5 P0 P3 P5 P20 Adult
E
Layer VI to VZ distance (μm)
E18.5 P4 P14 P28
F
E18.5
P4
P14
P28
Ctip2

Fig. 5

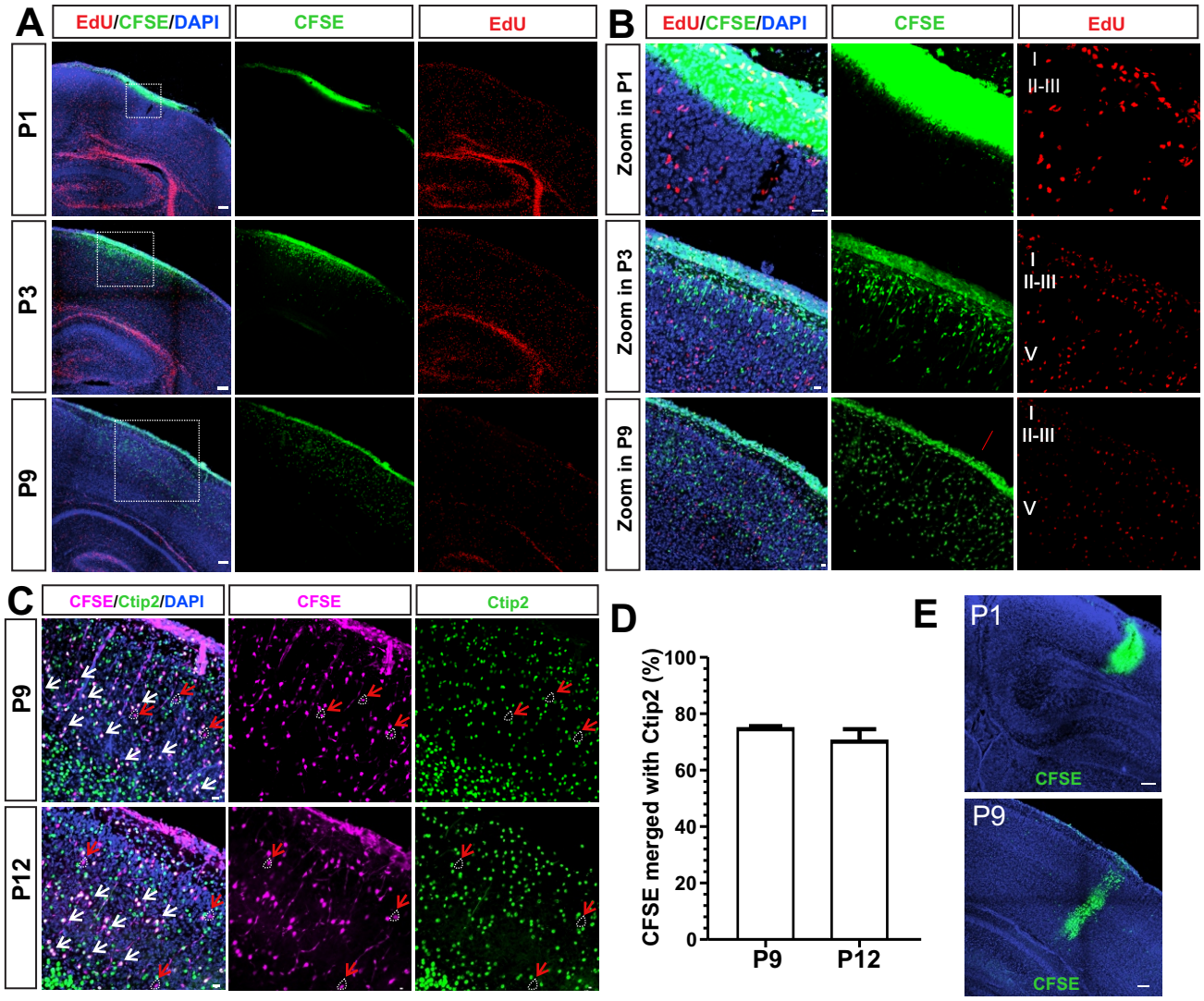
A
EdU/CFSE/DAPI
CFSE
EdU
P1
P3
P9
B
EdU/CFSE/DAPI
CFSE
EdU
Zoom in P1
Zoom in P3
Zoom in P9
I
II-III
V
C
CFSE/Ctip2/DAPI
CFSE
Ctip2
P9
P12
D
CFSE merged with Ctip2 (%)
100
80
60
40
20
0
P9
P12
E
P1
CFSE
P9
CFSE

Fig. 6

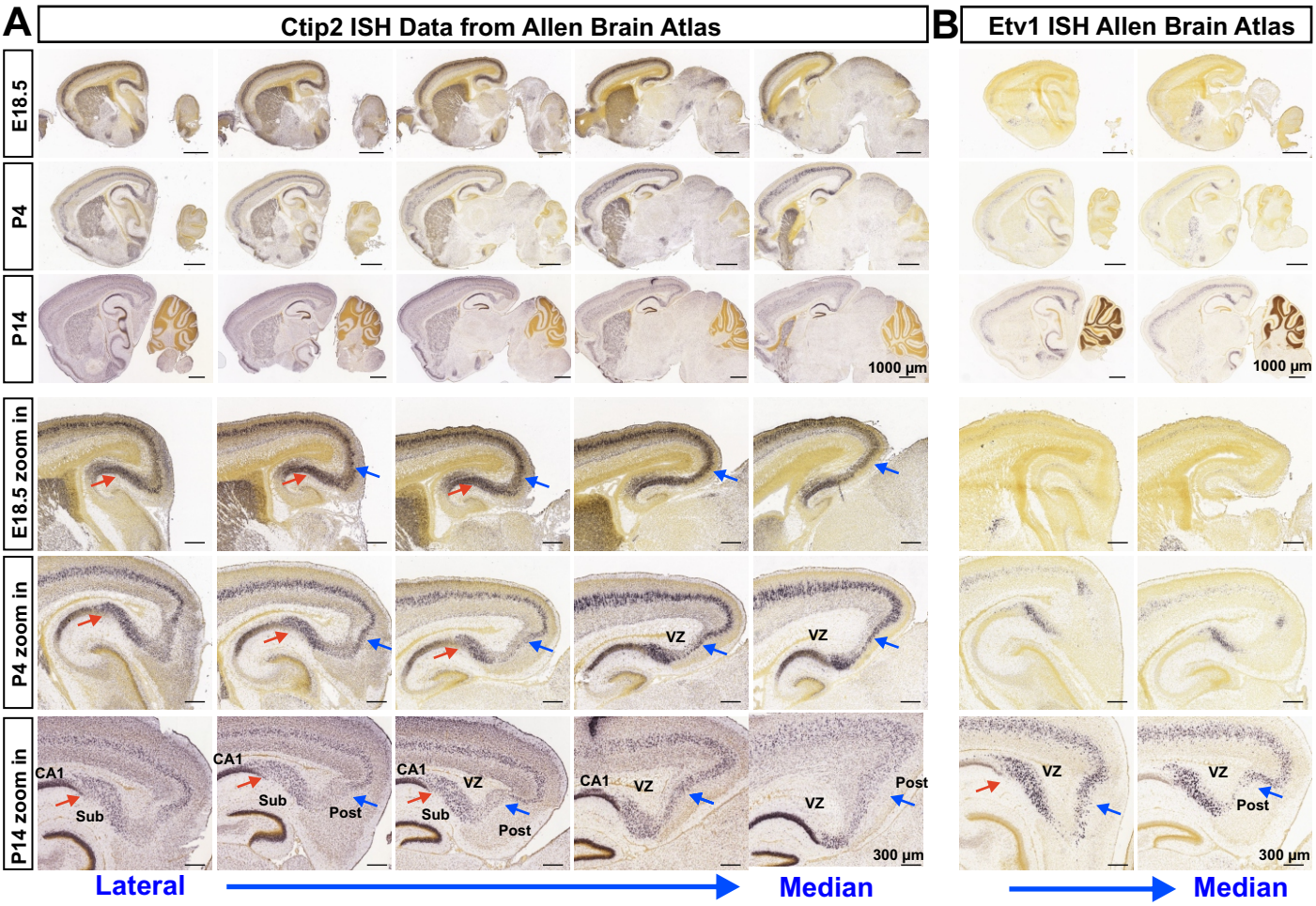
A
Ctip2 ISH Data from Allen Brain Atlas
B
Etv1 ISH Allen Brain Atlas
E18.5
P4
P14
1000 µm
E18.5 zoom in
P4 zoom in
P14 zoom in
CA1
Sub
Post
VZ
300 µm
Lateral
Median
Median

Fig.S7

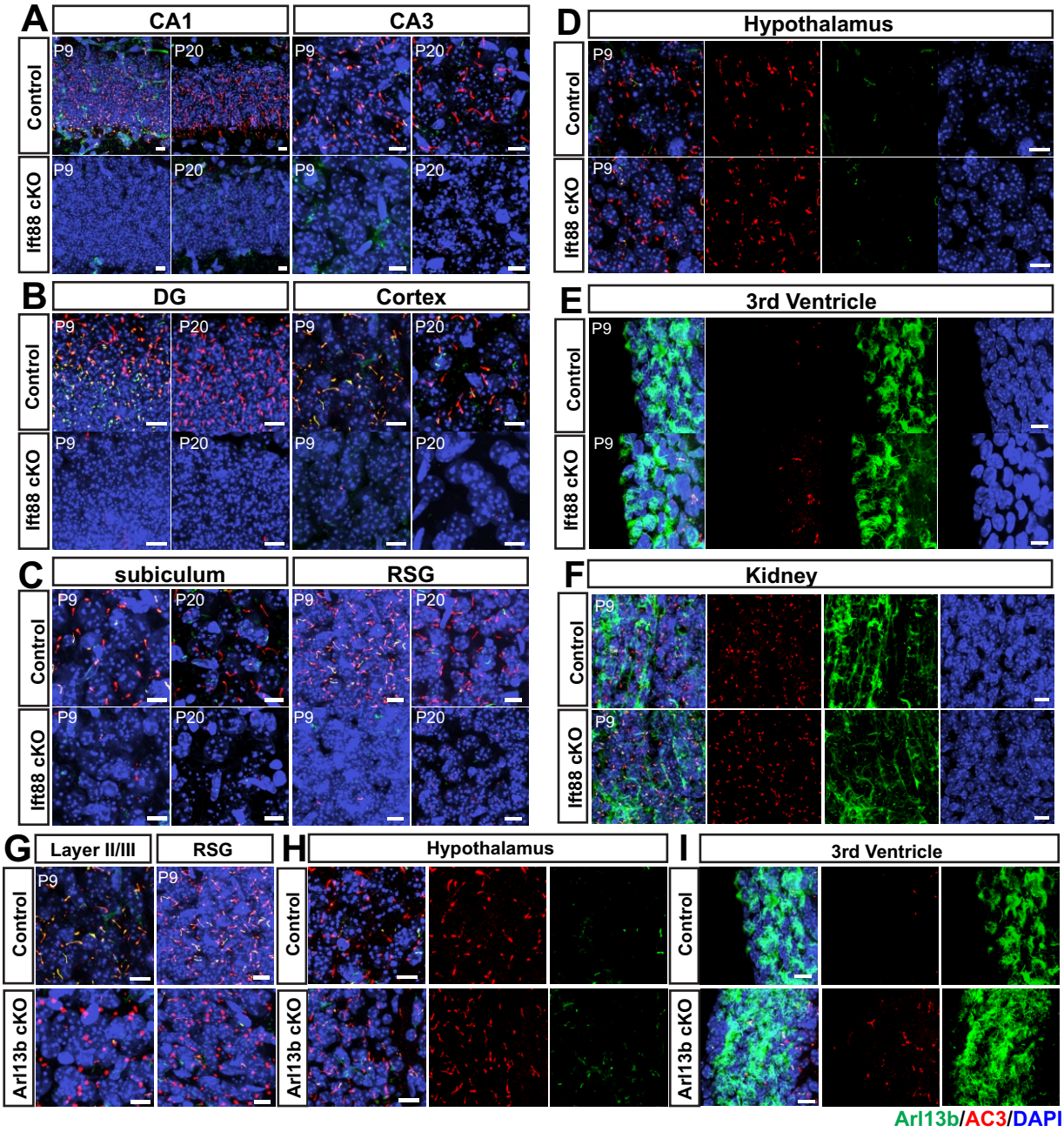
A
CA1
CA3
Control
Ift88 cKO
P9
P20
B
DG
Cortex
C
subiculum
RSG
D
Hypothalamus
E
3rd Ventricle
F
Kidney
G
Layer II/III
RSG
H
Hypothalamus
I
3rd Ventricle
Arl13b cKO
Arl13b/AC3/DAPI

Fig.S8

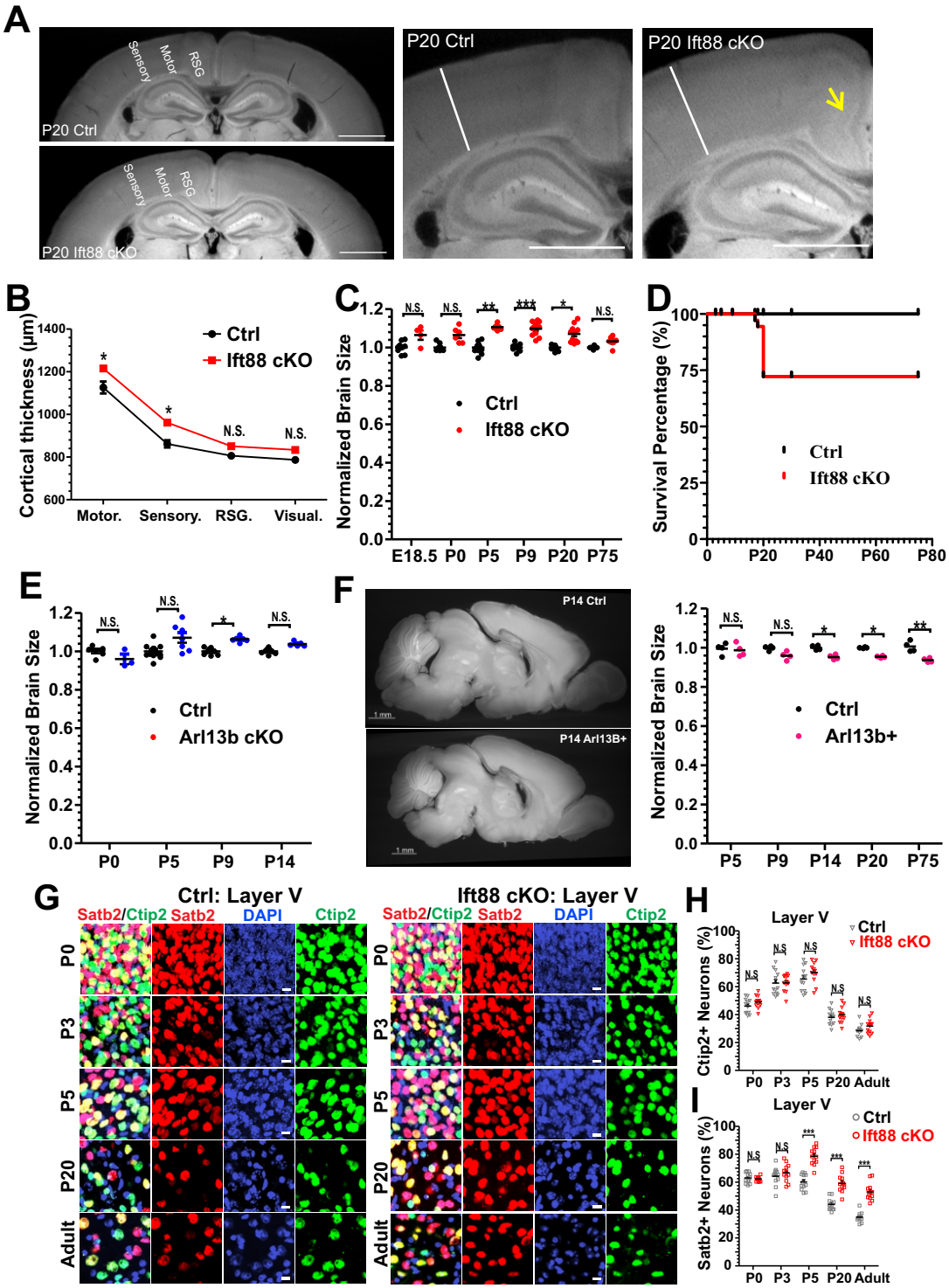
A
Sensory
Motor
RSG
P20 Ctrl
P20 Ift88 cKO
B
Cortical thickness (μm)
Ctrl
Ift88 cKO
Motor.
Sensory.
RSG.
Visual.
N.S.
C
Normalized Brain Size
E18.5
P0
P5
P9
P20
P75
D
Survival Percentage (%)
E
Arl13b cKO
F
P14 Ctrl
P14 Arl13B+
Arl13b+
G
Ctrl: Layer V
Ift88 cKO: Layer V
Satb2/Ctip2
Satb2
DAPI
Ctip2
Adult
H
Layer V
Ctip2+ Neurons (%)
I
Satb2+ Neurons (%)

Fig. 7

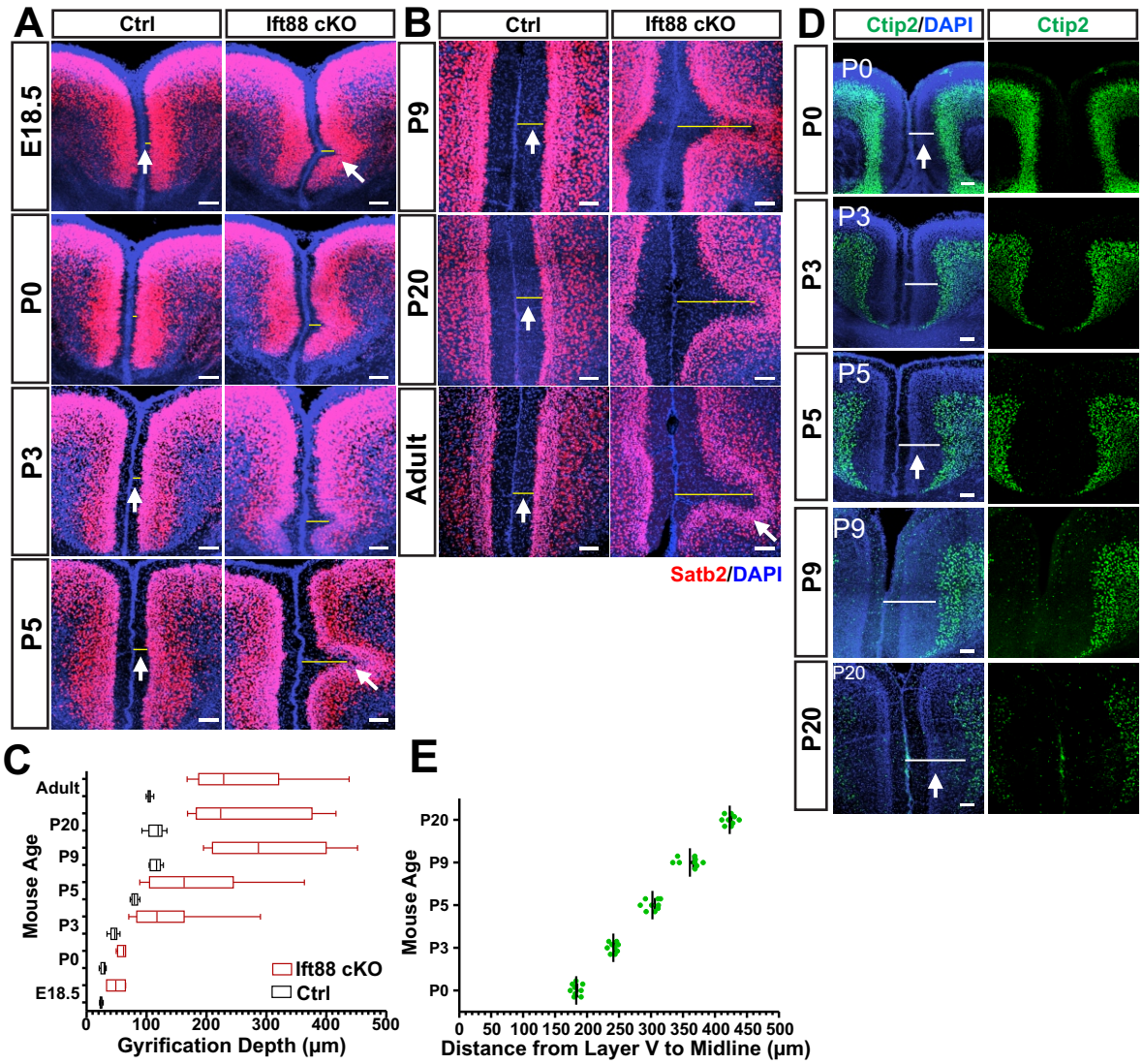
A
Ctrl
Ift88 cKO
E18.5
P0
P3
P5
B
Ctrl
Ift88 cKO
P9
P20
Adult
Satb2/DAPI
D
Ctip2/DAPI
Ctip2
P0
P3
P5
P9
P20
C
Adult
P20
P9
P5
P3
P0
E18.5
Mouse Age
Ift88 cKO
Ctrl
0
100
200
300
400
500
Gyrification Depth (μm)
E
P20
P9
P5
P3
P0
Mouse Age
0
50
100
150
200
250
300
350
400
450
500
Distance from Layer V to Midline (μm)

Fig. 8

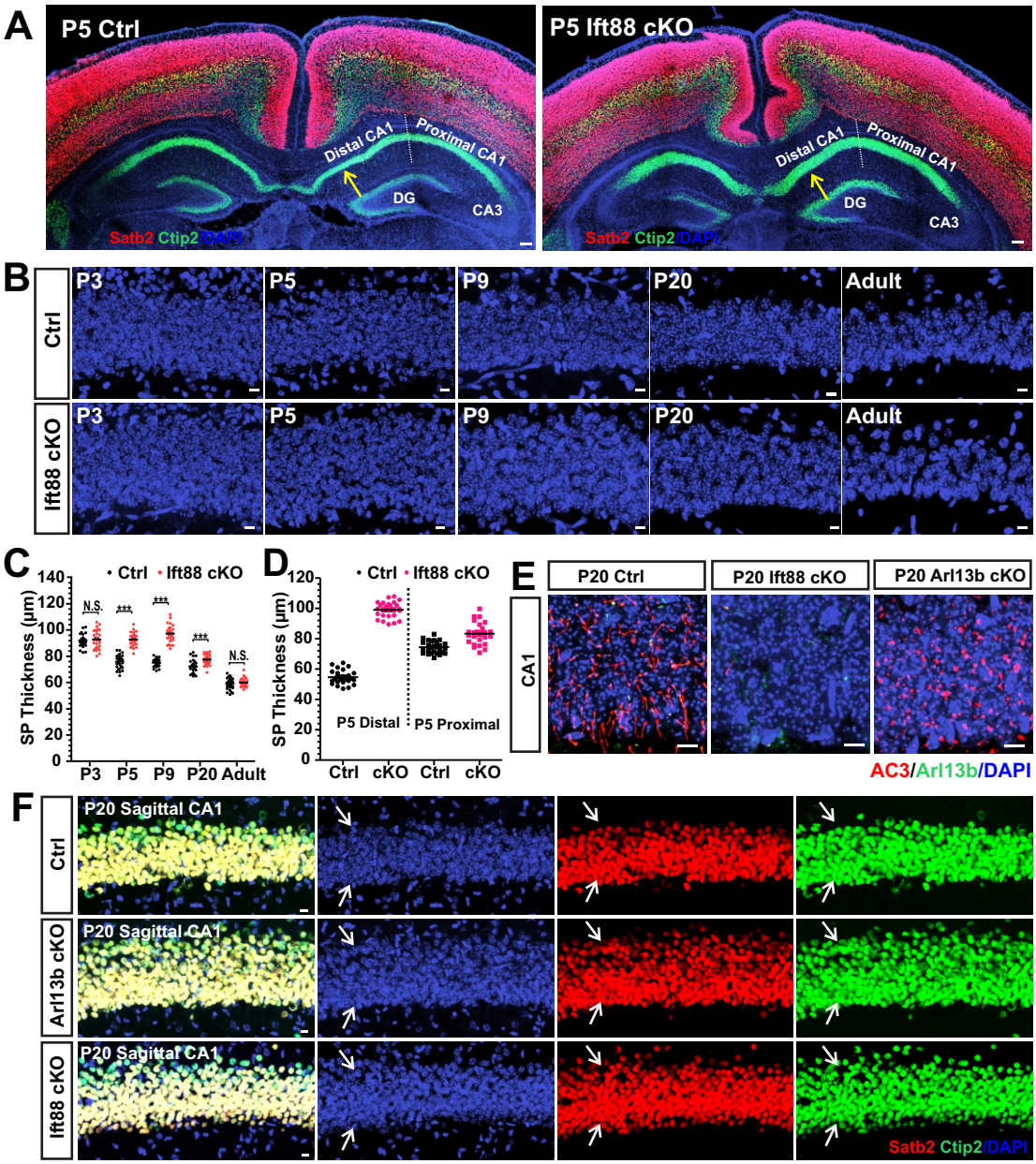
A
P5 Ctrl
P5 Ift88 cKO
Distal CA1
Proximal CA1
DG
CA3
Satb2 Ctip2/DAPI
B
Ctrl
Ift88 cKO
P3
P5
P9
P20
Adult
C
• Ctrl • Ift88 cKO
SP Thickness (μm)
N.S.
***
P3 P5 P9 P20 Adult
D
• Ctrl • Ift88 cKO
SP Thickness (μm)
P5 Distal
P5 Proximal
Ctrl cKO Ctrl cKO
E
P20 Ctrl
P20 Ift88 cKO
P20 Arl13b cKO
CA1
AC3/Arl13b/DAPI
F
Ctrl
Arl13b cKO
Ift88 cKO
P20 Sagittal CA1
Satb2 Ctip2/DAPI

Fig. 9

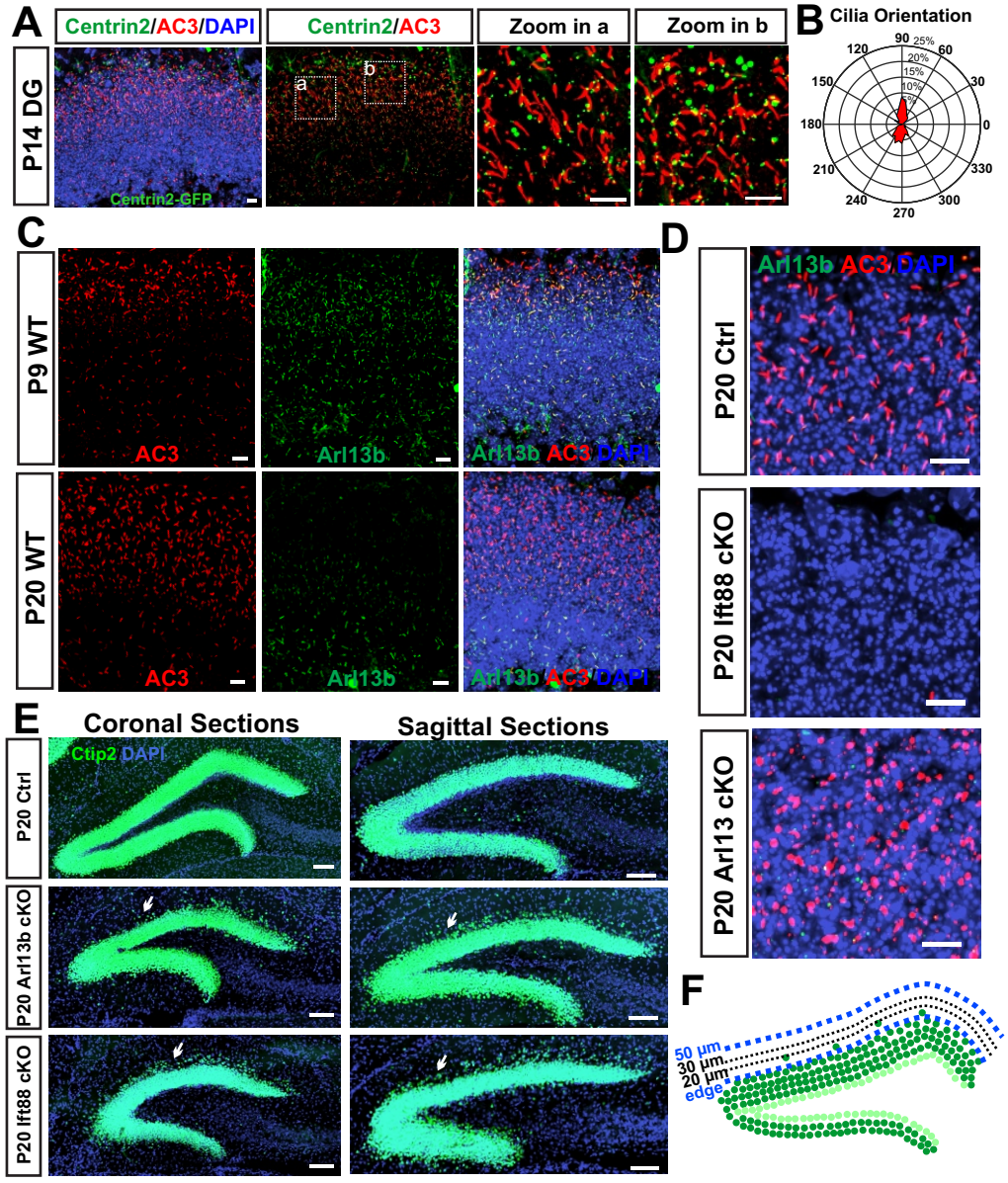
A
Centrin2/AC3/DAPI
Centrin2/AC3
Zoom in a
Zoom in b
P14 DG
Centrin2-GFP
a
b
B
Cilia Orientation
C
P9 WT
P20 WT
AC3
Arl13b
Arl13b AC3 DAPI
D
P20 Ctrl
P20 Ift88 cKO
P20 Arl13 cKO
E
Coronal Sections
Sagittal Sections
Ctip2 DAPI
P20 Ctrl
P20 Arl13b cKO
P20 Ift88 cKO
F
50 µm
30 µm
20 µm
edge
G
Coronal View
Sagittal View
Ctip2 Cells
P20 Ctrl
P20 Ift88 cKO
P20 Arl13b cKO
edge-20µm
20-30µm
30-50µm
edge-50µm
N.S.

Fig. 10

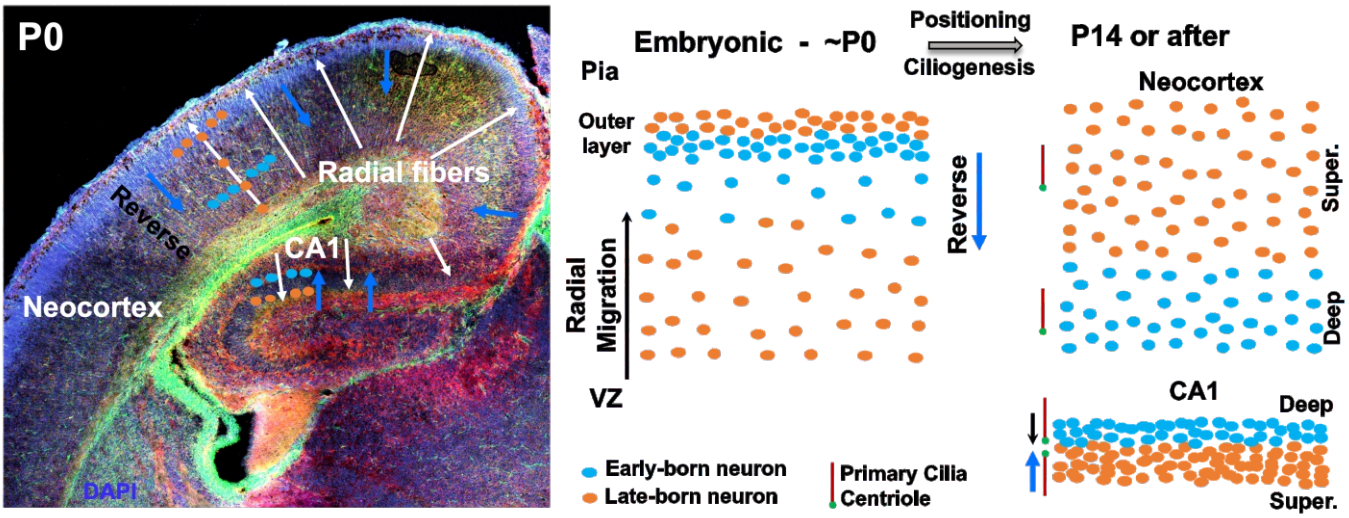
P0
Radial fibers
Reverse
CA1
Neocortex
DAPI
Embryonic - ~P0
Positioning
Ciliogenesis
P14 or after
Pia
Outer layer
Radial Migration
VZ
Reverse
Neocortex
Super.
Deep
CA1
Deep
Super.
Early-born neuron
Late-born neuron
Primary Cilia
Centriole

Fig. S9